NASA-CR-197014

UNIVERSITY OF ALABAMA IN HUNTSVILLE RESEARCH GRANT

ANNUAL REPORT ON

NUMERICAL STUDIES OF THE SURFACE TENSION EFFECT

OF CRYOGENIC LIQUID HELIUM

Research Grant Number:

NASA Research Grant NAG8-938

(NASA-CR-197014) NUMERICAL STUDIES OF THE SURFACE TENSION EFFECT OF CRYOGENIC LIQUID HELIUM Annual Report, period ending 30 Sep. 1994 (Alabama Univ.) 62 p

N95-14104

Unclas

G3/34 0028460

Prepared by

R. J. Hung, Ph.D.

Professor of Mechanical and Aerospace Engineering

The University of Alabama in Huntsville

Huntsville, Alabama 35899

October 1994

The University
Of Alabama
In Huntsville

Huntsville, Alabama 35899
(205) 895-6000
Telefax: (205) 895-6677

Research Administration

October 25, 1994

National Aeronautics and Space Administration
George C. Marshall Space Flight Center
ATTN: Mr. John Kaufmann/ES44
Marshall Space Flight Center, AL 35812

RE: Annual Report
NAG8-938

Dear Mr. Kaufmann:

Enclosed please find one (1) copy of the annual report for the period ending September 30, 1994, as required by NHB 5800.1C, for the above referenced grant. Additional distribution has been made as indicated below.

If you have any questions or need any additional information, please contact Mary L. [illegible] above number.

Table of Contents

	Pages
Abstract	i
I. Introduction	1
II. Functions of Scientific Observation and Spacecraft Motions	5
[illegible] of Gravity Gradient and Gravity	7
	18
stem	20
Fluid	26
	29
	37
erating	38
	47
	48
	54

Abstract

The generalized mathematical formulation of sloshing dynamics for partially filled liquid of cryogenic superfluid helium II in dewar containers driven by both the gravity gradient and jitter accelerations applicable to scientific spacecraft which is eligible to carry out spinning motion and/or slew motion for the purpose to perform scientific observation during the normal spacecraft operation are investigated. An example is given with Gravity Probe-B (GP-B) spacecraft which is responsible for the sloshing dynamics. The jitter accelerations include slew motion, spinning motion, atmospheric drag on the spacecraft, spacecraft attitude motions arising from machinery vibrations, thruster firing, pointing control of spacecraft, crew motion, etc. Explicit mathematical expressions to cover these forces acting on the spacecraft fluid systems are derived. The numerical computation of sloshing dynamics have been based on the non-inertia frame spacecraft bound coordinate, and solve time-dependent, three-dimensional formulations of partial differential equations subject to initial and boundary conditions. The explicit mathematical expressions of boundary conditions to cover capillary force effect on the liquid-vapor interface in microgravity environments are also derived. The formulations of fluid moment and angular moment fluctuations in fluid profiles induced by the sloshing dynamics, together with fluid stress and moment fluctuations exerted on the spacecraft dewar containers have been derived. Results of this study have been widely published in the open journals.

I. Introduction

For the purpose to carry out scientific experiments, some experimental spacecraft use cryogenic cooling for observation instrumentation and telescope, superconducting sensors for gyro read-out and maintain very low temperature near absolute zero for mechanical stability. The approaches to both cooling and control involve the use of superfluid liquid helium II. In this study, sloshing dynamics associated with spinning motions are investigated. To cover the spacecraft spinning motions, the Gravity Probe-B (GP-B) spacecraft has been chosen as the example in this study. The GP-B spacecraft adopts the cooling and boil-off from the cryogenic liquid helium dewar as a cryogen and propellant to maintain the cooling of instrumentations, attitude control and drag-free operation of the spacecraft. The potential problems for cryogenic liquid in dewar container could be due to asymmetry in the static liquid helium distribution and to perturbations in the liquid-vapor interface caused by slosh wave excitation driven by pointing control, machinery vibration, etc.

For the case of the GP-B spacecraft, cryogenic liquid helium II, at a temperature of 1.8 K, is used as the propellant. With its superconducting behavior, there is no temperature gradients in the liquid helium. In the absence of temperature gradient along the surface which drive Marangoni convection, the equilibrium shape of the free surface is governed by a balance of capillary, centrifugal and gravitational forces. Determination of liquid-vapor interface profiles based on computational experiments can uncover details of the flow which can not be easily visualized or measured experimentally in a microgravity environment.

The instability of the liquid-vapor interface surface can be induced by the presence of longitudinal and lateral accelerations. Slosh waves are, thus,

excited which produces high and low frequency oscillations in the liquid propellant. The sources of the residual accelerations range from the effects of the Earth's gravity gradient and jitter accelerations which include, atmospheric drag on the spacecraft, vibration of compressor, spacecraft attitude motions arising from machinery vibrations, thruster firings, spacecraft slew motion, pointing control of spacecraft, crew motion, etc. Recent study (Kamotani et al., 1981) suggest that the high frequency accelerations may be unimportant in comparison to the residual motions caused by low frequency accelerations.

Time-dependent dynamical behavior of partially-filled rotating fluids in reduced gravity environments was simulated by numerically solving the Navier Stokes equations subject to the initial and the boundary conditions (Hung and Shyu, 1991 a,b,c; 1992 a,b,c; Hung et al., 1991 a,b,c; 1992 a,b,c). At the interface between the liquid and the gaseous fluids, both the kinematic surface boundary condition, and the interface stress conditions for components tangential and normal to the interface, were applied (Hung and Shyu, 1991 a,b,c; 1992 a,b,c; Hung et al., 1991 a,b,c; 1992 a,b,c). The initial conditions were adopted from the steady-state formulations developed by Hung et al (1989 a,b,c). Some of the steady-state formulations of interface shapes were compared with the available experiments carried out by Leslie (1985) in a free-falling aircraft (KC-135). The experiments carried out by Mason et al (1978) showed that the classical fluid mechanics theory is applicable for cryogenic liquid helium in large containers.

In the spacecraft orbit around the Earth, the direction of azimuth angle of Earth toward the location of the spacecraft geometric center varies from 0° along the rolling axis of spacecraft to various directions in which three dimensional calculation shall be assumed.

As the spacecraft moves along the orbit, any fluid capable of motion

relative to the spacecraft is subject to the acceleration that arises from the gravity gradients of the Earth (Avduyevsky, 1984; Forward, 1982; Misner et al., 1973). The interaction between the particle mass of fluid and the spacecraft mass due to gravity gradient accelerations (Forward, 1982) are capable for the excitation of slosh waves and disturb the fluid system which induces the fluctuations of viscous stress and its moment exerted on the containers of the spacecraft fluid systems. In the meanwhile, the sources of residual acceleration of gravity jitter range from atmospheric drag on the spacecraft, background gravity, spacecraft attitude motions arising from machinery vibrations, spacecraft slew motion, thruster firings, crew motion, etc., are also capable for the excitation of slosh waves on the fluid containers.

It is critically important to understand the physical and dynamical behavior of cryogenic helium in a rotating cylinder to effectively promote space-oriented missions.

At temperatures close to absolute zero, quantum effects begin to be of importance in the properties of fluids. At a temperature of 2.17°K, liquid helium has a λ-point (a second-order phase transition); at temperatures below this point liquid helium (helium II) has a number of remarkable properties, the most important of which is superfluidity. This is the property of being able to flow without viscosity in narrow capillaries or gaps.

The basis of the dynamics of helium II is the following fundamental result of microscopic theory. At temperatures other than zero, helium II behaves as if it were a mixture of two different liquids. One of these is a superfluid and moves with zero viscosity along a solid surface. The other is a normal viscous fluid. It is of great importance that no friction occurs between these two parts of the liquid in their relative motion, i.e., no momentum is transferred from one

to the other.

It should be emphasized that regarding the liquid as a mixture of normal and superfluid parts is no more than a convenient description of the phenomena which occur in a fluid where quantum effects are important. One of these motions is normal and has the same properties as the motion of an ordinary viscous fluid, but the other is the motion of a superfluid. The two motions occur without any transfer of momentum from one to another. We can, in a certain sense, speak of the superfluid and normal parts of the fluid, but this does not mean that the fluid can actually be separated into two such parts.

If fluid flow can separate helium II into the regions of the superfluid and the normal fluid, two temperatures zones are immediately created. A very low temperature zone is located at the zone of very high density concentration of the superfluid, while a high temperature (below 2.17° K) zone is located at the zone of very high density concentration of the normal fluid at the other end. The existence of a sharp temperature gradient at the interface between the superfluid and the normal fluid results in the creation of a great difference in chemical potential, which, in turn, induces a great reverse pressure gradient, creating the environment of isothermal fluid distribution everywhere throughout the cylinder and homogenous distribution of superfluid density concentration. This illustration of the possible separation of superfluid from normal fluid of helium II means that there is in reality, no way for anyone to achieve the separation of the superfluid from the normal fluid of helium II. In other words, in considering the dynamical behavior of helium II in a large rotating cylinder, a mixture of the superfluid and the normal fluid without separation of the two fluids is accounted for in the model computation. Density concentration of superfluid is a function of temperature, which is also true for the surface

tension and viscous coefficient for helium II (Wilks, 1967; Hoare et al., 1961; Hung, 1990; Hung and Lee, 1992). In fact, the experiments carried out by Mason et al. (1978) showed that the classical fluid mechanics theory is applicable for cryogenic liquid helium in a large container. In this study, the theory of viscous Newtonian fluids is employed with modification of transport coefficients adjusted by normal and superfluid density concentration which is a function of temperature.

II. Functions of Scientific Observation and Spacecraft Motions

The GP-B spacecraft is a sun synchronous Earth satellite orbiting at 650 km altitude directly over the poles. The functions of scientific observation for the GP-B spacecraft and its motions are illustrated as follows:

The GP-B spacecraft is a relativity gyroscope experiment to test two extraordinary, universified predictions of Albert Einstein's general theory of relativity (Wilkinson et al., 1986; Stanford Relativity Gyroscope Experiment, 1986). By using gyroscopes (ones with electrically supported spheres, spinning in a vacuum and others which utilize the spins of atomic nuclei, circulating sound waves, and even circulating laser beams), the GP-B measures two distinct space-time processes, frame dragging and the geodetic effect, which gradually changes its directions of spin. In these gyroscopes, the underlying principle is that rotating systems, free from disturbing forces, should remain pointing in the same direction in space.

The physical meaning of "the same direction in space" can be explained from the differences in the Newtonian and Einsteinian concepts of the universe. For Newton, the answer was easy, in that space and time were absolutes. A perfect gyroscope set spinning and pointed at a star would stay aligned forever. Not so for Einstein, for whom space and time is warped. A gyroscope orbiting the Earth

finds two distinct space-time processes, frame dragging (rotation of space-time) and the geodetic effect (curvature of space-time), which will be measured by the GP-B.

As to frame-dragging for disturbances in the rotation of space-time, calculations based on a gyroscope in polar orbit at 650 km altitude should turn with the Earth through an angle amounting, after one year, to 42 milliarc-seconds (1 milliarc-second = 10^{-3} arc-second; 3.6 x 10^{3} arc-seconds = 1°, angular degree) (Everitt, 1990). As to the geodetic effect for disturbances in the curvature of space-time, the gyroscope's motion for rotation in the orbit plane at a 650 km altitude, from relativistic correction to the complicated motion of the Earth-Moon system around the Sun, should turn 6,600 milliarc-seconds per year (Everitt, 1990).

Furthermore, one of the GP-B's most important tasks is to investigate the gravitational action of moving matter in the universe. In other words, matter moving through space-time can be thought of as creating a new force-gravitomagnetism, which is similar to electromagnetic force created by an electric charge moving through magnetic fields (Misner et al., 1973; Everitt, 1990). The frame-dragging measurement detects this force and fixes its scale.

In order to insure these extremely precise and accurate measurements and gyroscope operations, near zero temperature is required for mechanical stability of the instrument, preservation of the lead bag magnetic shield, shielding the gyroscopes against nongravitation disturbances, and for reading their direction of spin. Near zero temperature cryogenic liquid helium II (1.8°K) has been chosen to serve this purpose (Mason et al., 1978; Hung, 1990).

The GP-B instrument comprises four gyroscopes and a reference telescope sighted on Rigel, a bright star in Orion. In polar orbit, with gyro spin

directions also pointing toward Rigel, the frame dragging and geodetic effects come out at right angles, each gyroscope measuring both. The GP-B attitude controller with a fine pointing system inside the dewar probe will constantly assure the operation of the spacecraft within the range of the scope of each experiment through the proper control of thrust.

Thrust comes freely from the dewar's boil-off helium vapor, in contrast to a traditional gas jet control system which uses on-off valves to save gas. Here, the copious supply of vapor allows the use of proportional thrusters: pairs of opposed nozzles adjusted continuously for much smoother control. Six thruster-pairs, suitably arrange, cover all three control functions with redundancy in case of failure. To take advantage of the characteristics of viscous-free superfluid helium II under λ transition point, a porous plug is used to control the helium boil-off and to produce the fountain pressure to serve as their thrust jet for the spacecraft propulsion system.

To comprise these functions of scientific observation, GP-B stores its gyroscopes, telescope, probe mass and others in the center core of the dewar probe surrounded by the cryogenic helium II liquid. The dewar container of the GP-B is spinning with a rotating rate of 0.1 rpm during normal operation. As the telescope is constantly sighted on Rigel, gyro spin directions also pointing toward Rigel during the spacecraft moving around the polar orbit. The GP-B with its rotating dewar, there is no slew motion involved in the spacecraft motion.

III. Basic Charcteristics of Gravity Gradient and Gravity Jitter Accelerations

Any fluid element inside the on-orbit spacecraft fluid system is subject to the acceleration that arises from the gravity gradient of the Earth (Avduyevsky, 1984; Forward, 1982; Misner et al., 1973; Hung and Pan, 1993; Hung

et al., 1993 a,b; 1994 a,b). Once the spacecraft orbit is fixed, the orbit period is determined and the basic structure of the gravity gradient acceleration also can be calculated. However, gravity gradient acceleration acting on each fluid element inside the on-orbit spacecraft fluid system is different dependent upon the distance of the location of the fluid element to the geometrical center of the spacecraft and its direction toward the location of the center of the Earth. This acceleration can only be calculated based on the non-inertia frame of spacecraft bound coordinate. Thus, the coordinate system shall be transformed from ordinary inertia frame coordinate to non-inertia coordinate.

(A) Orbit Motion of Spacecraft

Let us consider the case of the GP-B spacecraft, which is the Earth satellite orbiting at 650 km altitude directly over the poles, the orbit period, τ_o can be computed from following expression:

$$\tau_o = 2\pi \frac{R_c^{3/2}}{R_E g_o^{1/2}}$$

where R_E denotes the radius of Earth (= 6373 km); R_c, the radius of the circular orbit (= R_E + h = 7023 km); h, orbit altitude (= 650 km); and g_o, Earth gravity acceleration (= 9.81 $^m/s^2$). For the case of the GP-B spacecraft, the orbit period τ_o = 97.6 min, and orbit rate n = $^{2\pi}/\tau_o$ = 1.07 x 10^{-3} $^{rad}/_s$.

As the spacecraft is orbiting around the Earth, the azimuth angle of the Earth, ψ_E, toward the location of the spacecraft geometric center varies with respect to time. At time t = 0, the rolling axis of the spacecraft is aligned with the radial direction of the Earth's center to the spacecraft geometric center. Assuming the spacecraft rolling axis is linearly turning around 0° to 360° in the orbit period, τ_o, of the spacecraft when the spacecraft is orbiting around the Earth. This is particularly true for the case of the GP-B spacecraft.

Without the spacecraft slew motion, the azimuth angle (ψ_{E_o}) can be defined as

$$\psi_{E_o} = \frac{2\pi}{\tau_o} t \qquad (3\text{-}2)$$

where τ_o is the spacecraft orbit period [defined in Equation (3-1)]; and t is the time measured from the instant when the direction of the spacecraft rolling axis is aligned with the radial direction of the spacecraft geometric center to the center of the Earth.

(B) Spinning and Slew Motions of Spacecraft

For the purpose to carry out wide-range observations, some scientific spacecraft requires slew motion with respect to the mass center of the spacecraft. For the case of the spacecraft slew motion, azimuth angle, shown in Equation (3-2), shall be modified through the coordinate transformation of slew motion when the spacecraft is orbiting around the Earth.

Let us assume that the slew motion starts with the center located at the mass center of the spacecraft. Let us choose cartesian coordinate (x", y", z") with z"-axis along the axis of the dewar container (see Figure 1). At time t = 0, the radial vector $\hat{r}_c$ from the center of the spacecraft to the center of the Earth lies on the x"-z" plane of the cartesian coordinate chosen. The azimuth angle ψ_E is defined as the angle between the radial vector $\hat{r}_c$ and the z"-axis. Rotation matrices for spinning and/or slew motions along the x"-, y"- and z"-axes can be expressed as

$$\begin{bmatrix} 1 & 0 & 0 \\ 0 & \cos\omega_x t & \sin\omega_x t \\ 0 & -\sin\omega_x t & \cos\omega_x t \end{bmatrix}, \begin{bmatrix} \cos\omega_y t & 0 & -\sin\omega_y t \\ 0 & 1 & 0 \\ \sin\omega_y t & 0 & \cos\omega_y t \end{bmatrix}, \begin{bmatrix} \cos\omega_z t & \sin\omega_z t & 0 \\ -\sin\omega_z t & \cos\omega_z t & 0 \\ 0 & 0 & 1 \end{bmatrix}$$

respectively. Here, ω_x, ω_y and ω_z denote angular velocity of slew and/or spinning motions along the x"-, y"- and z"-axes, respectively. Radial vector $\hat{r}_c$

in cartesian coordinate without slew and spinning motion is

$$\hat{r}_{co} = [\sin\psi_{Eo}, 0, -\cos\psi_{Eo}] \tag{3-3}$$

With an execution of spinning motion along the z"-axis only, radial vector $\hat{r}_c$ becomes

$$\hat{r}_{c-z} = \begin{bmatrix} \cos\omega_z t & \sin\omega_z t & 0 \\ -\sin\omega_z t & \cos\omega_z t & 0 \\ 0 & 0 & 1 \end{bmatrix} \begin{bmatrix} \sin\psi_{Eo} \\ 0 \\ -\cos\psi_{Eo} \end{bmatrix}$$

$$= [\sin\psi_{Eo}\cos\omega_z t, -\sin\psi_{Eo}\sin\omega_z t, -\cos\psi_{Eo}] \tag{3-4}$$

With an execution of slew motion along the y"-axis only, radial vector $\hat{r}_c$ becomes

$$\hat{r}_{c-y} = \begin{bmatrix} \cos\omega_y t & 0 & -\sin\omega_y t \\ 0 & 1 & 0 \\ \sin\omega_y t & 0 & \cos\omega_y t \end{bmatrix} \begin{bmatrix} \sin\psi_{Eo} \\ 0 \\ -\cos\psi_{Eo} \end{bmatrix}$$

$$= [\sin(\psi_{Eo}+\omega_y t), 0, -\cos(\psi_{Eo}+\omega_y t)] \tag{3-5}$$

With an operation of slew motion along the x"-axis only, radial vector $\hat{r}_c$ becomes

$$\hat{r}_{c-x} = \begin{bmatrix} 1 & 0 & 0 \\ 0 & \cos\omega_x t & \sin\omega_x t \\ 0 & -\sin\omega_x t & \cos\omega_x t \end{bmatrix} \begin{bmatrix} \sin\psi_{Eo} \\ 0 \\ -\cos\psi_{Eo} \end{bmatrix}$$

$$= [\sin\psi_{Eo}, -\cos\psi_{Eo}\sin\omega_x t, -\cos\psi_{Eo}\cos\omega_x t] \tag{3-6}$$

In other words, radial vector $\hat{r}_c$ will be modified from the mathematical expression shown in Equation (3-3) to (3-4), (3-5) and (3-6) for the slew and/or spinning motions along the z"-, y"-, and x"-axes alone, respectively. In particular, for the case of slew motion along the y"-axis, comparison between Equations (3-3) and (3-5), it shows that the azimuth angle will be modified as

$$\psi_E = \psi_{Eo} + \omega_y t \tag{3-7}$$

For the successive operations of the spacecraft from spinning motion along the z"-axis, then slew motion along the y"-axis, and then slew motion along the x"-axis, radial vector $\hat{r}_c$ results

$$\mathcal{L}_{c\text{-}z,y,x} = \begin{bmatrix} 1 & 0 & 1 \\ 0 & \cos\omega_x t & \sin\omega_x t \\ 0 & -\sin\omega_x t & \cos\omega_x t \end{bmatrix} \begin{bmatrix} \cos\omega_y t & 0 & -\sin\omega_y t \\ 0 & 1 & 0 \\ \sin\omega_y t & 0 & \cos\omega_y t \end{bmatrix} \cdot$$

$$\cdot \begin{bmatrix} \cos\omega_z t & \sin\omega_z t & 0 \\ -\sin\omega_z t & \cos\omega_z & 0 \\ 0 & 0 & 1 \end{bmatrix} \begin{bmatrix} \sin\psi_{Eo} \\ 0 \\ -\cos\psi_{Eo} \end{bmatrix} \tag{3-8}$$

In addition to the modification of the azimuth angle made by the spacecraft slew motion through the formulation of coordinate transformation, shown in Equation (3-3) to (3-8), accelerations are also induced to activate on the fluid mass in the dewar container. Accelerations acting on the fluid particle in the dewar induced by the slew motion of the spacecraft with the coordinate fixed at the spacecraft center of the mass is as follows (see Figure 1):

$$\ddot{\vec{R}}_p = \vec{\omega} x (\vec{\omega} x \vec{R}_p) + \vec{\alpha} x \vec{R}_p + 2\vec{\omega} x \vec{v} \tag{3-9}$$

where $\vec{R}_p$ denotes the position vector of the fluid particle in the dewar container relative to the body frame of the spacecraft; $\vec{\omega}$, angular velocity of the spacecraft body frame; $\vec{\alpha}$, angular acceleration of the spacecraft body frame; and $\vec{v}$, velocity of the fluid particle relative to the spacecraft body frame.

As we indicated earlier, let us assume that the slew motion starts with the center located at the spacecraft mass center, cartesian coordinate (x'', y'', z'') is chosen with origin located at the spacecraft mass center. Let us also assume that x''-z'' plane intersects the center of Earth and the spacecraft mass

center. In other words, azimuth angle of Earth toward the spacecraft mass center lies in the x''-z'' plane. Slew motion is along both the x''- and y''-coordinates. Thus, $\vec{\omega}_s = (\omega_{sx}, \omega_{sy}, 0)$ and $\vec{\alpha}_s = (\alpha_{sx}, \alpha_{sy}, 0)$, $\ddot{\vec{R}}_p$ due to slew motion becomes

$$\ddot{\vec{R}}_{p,\,slew} = \begin{bmatrix} \ddot{R}_{x''} \\ \ddot{R}_{y''} \\ \ddot{R}_{z''} \end{bmatrix}_{slew} = \begin{bmatrix} \omega_{sy}(\omega_{sx}R_y - R_x\omega_{sy}) + \alpha_{sy}R_z + 2\omega_{sy}V_z \\ -\omega_{sx}(\omega_{sx}R_y - R_x\omega_{sy}) - \alpha_{sx}R_z - 2\omega_{sx}V_z \\ -R_z(\omega_{sx}^2 + \omega_{sy}^2) + (\alpha_{sx}R_y - \alpha_{sy}R_x) + 2(\omega_{sx}V_y - \omega_{sy}V_x) \end{bmatrix}_{slew}$$

(C) Coupling for the Accelerations of Spinning and Slew Motion of Spacecraft

For some particular reasons required in the scientific spacecraft, it might be faced with the situation that both spinning and slew motions are needed simultaneously. To encounter this case, the following formulations are made to deal with coupling for the accelerations of spinning and slew motion of the spacecraft:

$$\ddot{\vec{R}}_{p,\,slew\ and\ spinning} = \begin{bmatrix} \ddot{R}_x \\ \ddot{R}_y \\ \ddot{R}_z \end{bmatrix}_{slew\ and\ spinning}$$

$$= \begin{bmatrix} \omega_{sy}(\omega_{sx}R_y - \omega_{sy}R_x) + \alpha_{sy}R_z + 2\omega_{sy}V_z \\ -\omega_{sx}(\omega_{sx}R_y - \omega_{sy}R_x) - \alpha_{sx}R_z - 2\omega_{sx}V_z \\ -R_z(\omega_x^2 + \omega_{sy}^2) + (\alpha_{sx}R_y - \alpha_{sy}R_x) + 2(\omega_{sx}V_y - \omega_{sy}V_x) \end{bmatrix}_{slew}$$

$$+ \begin{bmatrix} -(\omega_z R_x - \omega_{sx}R_z)\omega_z - \dot{\omega}_z R_y - 2\omega_z V_y \\ (\omega_{sy}R_z - \omega_z R_y)\omega_z + \dot{\omega}_z R_x + 2\omega_z V_x \\ (\omega_{sx}R_x + \omega_{sy}R_y)\omega_z \end{bmatrix}_{spinning\ and\ coupling} \qquad (3\text{-}11)$$

where ω_z and $\dot{\omega}_z$ denote angular velocity and angular acceleration, respectively, of spacecraft spinning motion along the z-axis.

For the case of the GP-B spacecraft, there is no slew motion and the

spinning is the only acceleration acting on the spacecraft fluid system. Acceleration due to spacecraft spinning motion becomes

$$\ddot{\vec{R}}_{p,\,spinning} = \begin{bmatrix} \ddot{\vec{R}}_x \\ \ddot{\vec{R}}_y \\ \ddot{\vec{R}}_z \end{bmatrix}_{spinning} = \begin{bmatrix} -R_x\omega_z^2 - R_y\dot{\omega}_z - 2\omega_z V_y \\ -R_y\omega_z^2 + R_x\dot{\omega}_z + 2\omega_z V_x \\ 0 \end{bmatrix}_{spinning} \qquad (3\text{-}12)$$

To convert the expression of Equation (3-12) in cartesian coordinate to cylindrical coordinate, by using the relationships of $(R_x, R_y) = (r\cos\theta, r\sin\theta)$ and $(v_x, v_y) = (u_r\cos\theta - u_\theta\sin\theta, u_r\sin\theta + u_\theta\cos\theta)$, Equation (3-12) becomes

$$\ddot{\vec{R}}_{p,\,spinning} = \begin{bmatrix} \ddot{\vec{R}}_x \\ \ddot{\vec{R}}_y \\ \ddot{\vec{R}}_z \end{bmatrix}_{spinning} = \begin{bmatrix} -r\cos\theta\,\omega_z^2 - r\sin\theta\,\dot{\omega}_z - 2(u_r\sin\theta + u_\theta\cos\theta)\,\omega_z \\ -r\sin\theta\,\omega_z^2 + r\cos\theta\,\dot{\omega}_z + 2(u_r\cos\theta - u_\theta\sin\theta)\,\omega_z \\ 0 \end{bmatrix}_{spinning} \qquad (3\text{-}13)$$

and

$$\ddot{\vec{R}}_{p,\,spinning} = \begin{bmatrix} \ddot{\vec{R}}_r \\ \ddot{\vec{R}}_\theta \\ \ddot{\vec{R}}_z \end{bmatrix}_{spinning} = \begin{bmatrix} \ddot{\vec{R}}_x\cos\theta + \ddot{\vec{R}}_y\sin\theta \\ -\ddot{\vec{R}}_x\sin\theta + \ddot{\vec{R}}_y\cos\theta \\ \ddot{\vec{R}}_z \end{bmatrix}_{spinning} = \begin{bmatrix} -r\omega_z^2 - 2u_\theta\omega_z \\ r\dot{\omega}_z + 2u_r\omega_z \\ 0 \end{bmatrix}_{spinning} \qquad (3\text{-}14)$$

Accelerations induced by spacecraft spinning motion alone becomes

$$\begin{bmatrix} a_r \\ a_\theta \\ a_z \end{bmatrix}_{spinning} = -\begin{bmatrix} \ddot{\vec{R}}_r \\ \ddot{\vec{R}}_\theta \\ \ddot{\vec{R}}_z \end{bmatrix}_{spinning} = \begin{bmatrix} r\omega_z^2 + 2u_\theta\omega_z \\ -r\dot{\omega}_z - 2u_r\omega_z \\ 0 \end{bmatrix}_{spinning} \qquad (3\text{-}15)$$

(D) Gravity Gradient Acceleration

The gravity gradient acceleration acting on the fluid mass of spacecraft can be shown as

$$\hat{a}_{gg} = n^2\left[3\left(\hat{r}_c\cdot\hat{d}\right)\hat{r}_c - \hat{d}\right] \qquad (3\text{-}16)$$

where $\hat{a}_{gg}$ denotes gravity gradient acceleration vector; $\hat{d}$, the vector (not a unit vector) from the fluid element to the spacecraft geometric center; $\hat{r}_c$, a unit vector from the spacecraft geometric center to the center of the Earth; and n,

the orbit rate (see Figure 1).

It is assumed that the gravity gradient exerted on the geometrical center of the spacecraft orbiting around the Earth on its specified orbit is zero. In other words, all the gravity acceleration exerted on the spacecraft is nothing but the gravity gradient acceleration which is defined in Equation (3-16). In this study, we are interested in investigating how gravity gradient acceleration affects the dynamical behaviors of cryogenic fluid elements of helium.

For the convenience of mathematical calculation, let us describe all the parameters involved in Equation (3-16) in terms of cartesian coordinates. In order to match with the computer simulation, mathematical derivation are considered in the first quadrant. Figure 1 illustrates the geometrical relationship of the parameters shown in Equation (3-16).

Let us consider the fluid element of interests, m, located at (r, θ, z) in cylindrical coordinates and at (x, y, z) in cartesian coordinates. The origin of the two coordinate systems is located at the center bottom of the dewar tank. The slew and/or spinning motions, mentioned earlier, are executed at the spacecraft mass center with cartesian coordinate (x", y", z"). The geometry center or the spacecraft mass center is located at $z = L_c$. As $|\hat{d}|$ (not an unit vector) is much smaller than the distance between the location of the GP-B spacecraft geometric center to the center of the Earth, $\hat{r}_c$ (an unit vector) through the GP-B geometric center and $\hat{r}_c$ (an unit vector) through the fluid element, m, is basically the same. Assume that vector $\hat{r}_c$ lies in the x-z plane of the cartesian coordinate.

Radial vector $\hat{r}_c$ with the modification of slew and/or spinning motions along the x"-, y"-, z"-axes have been derived in Equations (3-3) to (3-8). Based on the relationship between coordinates (x, y, z) and (x", y", z")

$$\begin{bmatrix} x \\ y \\ z-L_c \end{bmatrix} = \begin{bmatrix} 1 & 0 & 0 \\ 0 & 1 & 0 \\ 0 & 0 & 1 \end{bmatrix} \begin{bmatrix} x'' \\ y'' \\ z'' \end{bmatrix} \tag{3-17}$$

Vector $\hat{d}$ in (x, y, z) coordinate becomes

$$\hat{d} = [-r\cos\theta, -r\sin\theta, -(z-L_c)] \tag{3-18}$$

Substituting Equations (3-4) and (3-18) in (3-16), non-inertia frame expression of gravity gradient acceleration with spinning motion in z-axis becomes

$$\begin{bmatrix} a_{gg,x} \\ a_{gg,y} \\ a_{gg,z} \end{bmatrix}_{spinning\ in\ z\text{-}axis} = n^2 \begin{bmatrix} 3[-r\sin\psi_{Eo}\cos(\theta+\omega_z t)+(z-L_c)\cos\psi_{Eo}]\sin\psi_{Eo}\cos\omega_z t + r\cos\theta \\ -3[-r\sin\psi_{Eo}\cos(\theta+\omega_z t)+(z-L_c)\cos\psi_{Eo}]\sin\psi_{Eo}\sin\omega_z t + r\sin\theta \\ -3[-r\sin\psi_{Eo}\cos(\theta+\omega_z t)+(z-L_c)\cos\psi_{Eo}]\cos\psi_{Eo} + (z-L_c) \end{bmatrix} \tag{3-19}$$

Substituting Equations (3-5) and (3-18) in (3-16), non-inertia frame expressions of gravity gradient acceleration with slew motion in y-axis becomes

$$\begin{bmatrix} a_{gg,x} \\ a_{gg,y} \\ a_{gg,z} \end{bmatrix}_{slew\ in\ y\text{-}axis} = n^2 \begin{bmatrix} 3[-r\sin\psi\cos\theta+\cos\psi(z-L_c)]\sin\psi + r\cos\theta \\ r\sin\theta \\ -3[-r\sin\psi\cos\theta+\cos\psi(z-L_c)]\cos\psi + (z-L_c) \end{bmatrix} \tag{3-20}$$

where $\psi_E = \psi_{Eo} + \omega_y t$.

Substituting Equations (3-6) and (3-18) in (3-16), non-inertia frame expressions of gravity gradient acceleration with slew motion in x-axis becomes

$$\begin{bmatrix} a_{gg,x} \\ a_{gg,y} \\ a_{gg,z} \end{bmatrix}_{slew\ in\ x\text{-}axis} = n^2 \begin{bmatrix} 3(-r\cos\theta\sin\psi_{Eo}+\cos\psi_{Eo}[r\sin\omega_x t\sin\theta+\cos\omega_x t(z-L_c)])\sin\psi_{Eo}+r\cos\theta \\ -3(-r\cos\theta\sin\psi_{Eo}+\cos\psi_{Eo})]\sin\omega_x t\sin\theta+\cos\omega_x t(z-L_c)]\cos\psi_{Eo}\sin\omega_x t+r\sin\theta \\ -3(-r\cos\theta\sin\psi_{Eo}+\cos\psi_{Eo}[r\sin\omega_x t\sin\theta+\cos\omega_x t(z-L_c)])\cos\psi_{Eo}\cos\omega_x t+(z-L_c) \end{bmatrix} \tag{3-21}$$

The relationship for the coordinate transformation from cartesian to cylindrical coordinates for any vector $\hat{F}$ (such as velocity or force vectors) in non-inertia frame of spacecraft bound coordinate can be shown as

$$\begin{bmatrix} F_r \\ F_\theta \\ F_z \end{bmatrix} = \begin{bmatrix} \cos\theta & \sin\theta & 0 \\ -\sin\theta & \cos\theta & 0 \\ 0 & 0 & 1 \end{bmatrix} \begin{bmatrix} F_x \\ F_y \\ F_z \end{bmatrix} \tag{3-22}$$

Thus, the gravity gradient acceleration located at (r, θ, z) can be computed from that located at (x, y, z), shown in Equations (3-18) to (3-21), from the following relation:

$$\hat{a}_{gg} = \begin{bmatrix} a_{gg,r} \\ a_{gg,\theta} \\ a_{gg,z} \end{bmatrix} = \begin{bmatrix} \cos\theta & \sin\theta & 0 \\ -\sin\theta & \cos\theta & 0 \\ 0 & 0 & 1 \end{bmatrix} \begin{bmatrix} a_{gg,x} \\ a_{gg,y} \\ a_{gg,z} \end{bmatrix} \tag{3-23}$$

(E) Jitter Accelerations

In addition to gravity gradient acceleration acting on the fluid element of on-orbit spacecraft fluid systems, there is another acceleration of gravity jitter also exerted forces on the fluid systems. The sources of residual acceleration of gravity jitter range from slew motion of spacecraft, atmospheric drag on the spacecraft, background gravity, spacecraft attitude motions arising from machinery vibrations, thruster firings, crew motion, etc., are also capable for the excitation of slosh waves in spacecraft fluid systems (Kamotani et al., 1981; Hung and Shyu, 1991 a,b,c; 1992 a,b,c; 1993 a,b; 1994 Hung et al., 1992 a,b; 1994).

Among all of the varieties of jitter accelerations listed, accelerations induced by slew motion of the spacecraft dominate the forces activated on the spacecraft fluid systems. Two coordinate systems (cylindrical and cartesian) chosen in this study are (r, θ, z) with corresponding velocity components (u_r, u_θ, u_z) for cylindrical, and (x, y, z) with corresponding velocity components (u_x, u_y, u_z) for cartesian coordinates. The origin of these two coordinates are located at the central bottom of the dewar tank, as shown in Figure 1. The

spacecraft center of mass, or the geometric center of the spacecraft is located at $(x_c, y_c, z_c) = (0, 0, L_c)$. The relationships of the coordinate, velocity and the force between cartesian and cylindrical coordinates are

$$\begin{bmatrix} x \\ y \\ z \end{bmatrix} = \begin{bmatrix} \cos\theta & 0 & 0 \\ \sin\theta & 0 & 0 \\ 0 & 0 & 1 \end{bmatrix} \begin{bmatrix} r \\ \theta \\ z \end{bmatrix} \tag{3-24}$$

$$\begin{bmatrix} u_x \\ u_y \\ u_z \end{bmatrix} = \begin{bmatrix} \cos\theta & -\sin\theta & 0 \\ \sin\theta & \cos\theta & 0 \\ 0 & 0 & 1 \end{bmatrix} \begin{bmatrix} u_r \\ u_\theta \\ u_z \end{bmatrix} \tag{3-25}$$

$$\begin{bmatrix} F_r \\ F_\theta \\ F_z \end{bmatrix} = \begin{bmatrix} \cos\theta & \sin\theta & 0 \\ -\sin\theta & \cos\theta & 0 \\ 0 & 0 & 1 \end{bmatrix} \begin{bmatrix} F_x \\ F_y \\ F_z \end{bmatrix} \tag{3-26}$$

In the derivation of acceleration induced by the slew motion of spacecraft, the coordinate system (x", y", z") is fixed at the spacecraft center of the mass. The relationships of the coordinate, velocity and acceleration between expressions with the origin located at the spacecraft center of the mass (x", y", z") and origin located at the center bottom of the dewar tank (x, y, z) are

$$\begin{bmatrix} R_x \\ R_y \\ R_z \end{bmatrix} = \begin{bmatrix} x \\ y \\ z-L_c \end{bmatrix} = \begin{bmatrix} \cos\theta & 0 & 0 \\ \sin\theta & 0 & 0 \\ 0 & 0 & 1 \end{bmatrix} \begin{bmatrix} r \\ \theta \\ z-L_c \end{bmatrix} \tag{3-27}$$

$$\begin{bmatrix} V_x \\ V_y \\ V_z \end{bmatrix} = \begin{bmatrix} u_x \\ u_y \\ u_z \end{bmatrix} = \begin{bmatrix} \cos\theta & -\sin\theta & 0 \\ \sin\theta & \cos\theta & 0 \\ 0 & 0 & 1 \end{bmatrix} \begin{bmatrix} u_r \\ u_\theta \\ u_z \end{bmatrix} \tag{3-28}$$

$$\begin{bmatrix} \ddot{R}_x \\ \ddot{R}_y \\ \ddot{R}_z \end{bmatrix}_{slew} = \begin{bmatrix} F_x \\ F_y \\ F_z \end{bmatrix}_{slew} = \begin{bmatrix} \cos\theta & \sin\theta & 0 \\ -\sin\theta & \cos\theta & 0 \\ 0 & 0 & 1 \end{bmatrix}^{-1} \begin{bmatrix} F_r \\ F_\theta \\ F_z \end{bmatrix}_{slew} \tag{3-29}$$

$$\begin{bmatrix} F_r \\ F_\theta \\ F_z \end{bmatrix}_{slew} = \begin{bmatrix} \cos\theta & \sin\theta & 0 \\ -\sin\theta & \cos\theta & 0 \\ 0 & 0 & 1 \end{bmatrix} \begin{bmatrix} F_x \\ F_y \\ F_z \end{bmatrix}_{slew} \qquad (3\text{-}30)$$

A detailed expression of $[\ddot{R}_x, \ddot{R}_y, \ddot{R}_z]_{slew}$ are shown in Equation (3-10) of this report. Jitter acceleration is a summation of acceleration induced by slew motion and others, such as atmospheric drag on the spacecraft, spacecraft attitude motions arising from machinery vibration, thruster firing, crew motion, etc. Thus, jitter acceleration can be expressed as

$$\hat{a}_{gj} = \begin{bmatrix} a_{gj,r} \\ a_{gj,\theta} \\ a_{gj,z} \end{bmatrix}_{slew} + \begin{bmatrix} a_{gj,r} \\ a_{gj,\theta} \\ a_{gj,z} \end{bmatrix}_{others} = -\begin{bmatrix} F_r \\ F_\theta \\ F_z \end{bmatrix}_{slew} - \begin{bmatrix} F_r \\ F_\theta \\ F_z \end{bmatrix}_{others} \{ 1 + \frac{1}{2}\sin(2\pi ft) \}$$

$$= -\begin{bmatrix} \cos\theta & \sin\theta & 0 \\ -\sin\theta & \cos\theta & 0 \\ 0 & 0 & 1 \end{bmatrix} \begin{bmatrix} F_x \\ F_y \\ F_z \end{bmatrix}_{slew} - \begin{bmatrix} F_r \\ F_\theta \\ F_z \end{bmatrix}_{others} \{ 1 + \frac{1}{2}\sin(2\pi ft) \} \qquad (3\text{-}31)$$

where f is the jitter frequency (Hz) imposed on the fluid systems of the spacecraft.

IV. Non-Inertia Frame Mathematical Formulation of Fundamental Equations

Dynamical behavior of fluid elements inside the on-orbit spacecraft fluid systems are strongly modified by the gravity gradient and gravity jitter accelerations. In order to accommodate the impact of gravity gradient acceleration, in particular, on the on-orbit fluid motion, one has to consider non-inertia frame of the spacecraft bound coordinate rather than adopting inertia frame coordinate used in ordinary fluid mechanics formulation.

Consider a closed circular cylindrical dewar of radius, a, with height, L, which is partially filled with cryogenic liquid helium, and rest of the ullage is filled with a helium vapor. Angular velocity of rotating cylinder is ω.

Density and viscosity of liquid helium and helium vapor are ρ_L, μ_L, ρ_v, and μ_v, respectively (Mason, 1978). Let us use cylindrical coordinates (r, θ, z), with corresponding velocity components (u, v, w), and corresponding residual gravity acceleration, such as gravity gradient components ($a_{gg,r}$, $a_{gg,\theta}$, $a_{gg,z}$) and gravity jitter components ($a_{gj,r}$, $a_{gj,\theta}$, $a_{gj,z}$). In the derivation of the governing equations, accelerations induced by the spinning motion of the spacecraft is included in the formulation. The rest of the acceleration such as slew motion, atmospheric drag on the spacecraft, spacecraft attitude motions arising from machinery vibrations, thruster firing and others, are included in the jitter acceleration, shown in Equation (3-31). The governing equations for non-inertia frame of spacecraft bound coordinates can be shown as follows:

(A) Continuity Equation

$$\frac{1}{r}\frac{\partial}{\partial r}(ru)+\frac{1}{r}\frac{\partial v}{\partial \theta}+\frac{\partial w}{\partial z}=0 \qquad (4\text{-}1)$$

(B) Momentum Equations

$$\rho\left(\frac{\partial u}{\partial t}+u\frac{\partial u}{\partial r}+\frac{v}{r}\frac{\partial u}{\partial \theta}-\frac{v^2}{r}+w\frac{\partial u}{\partial z}\right)=-\frac{\partial p}{\partial r}+2\rho\omega_z v+\rho\left(a_{gj,r}+a_{gg,r}\right)+\rho r\omega_z^2$$

$$+\mu\left(\nabla^2 u-\frac{u}{r^2}-\frac{2}{r^2}\frac{\partial v}{\partial \theta}\right) \qquad (4\text{-}2)$$

$$\rho\left(\frac{\partial v}{\partial t}+u\frac{\partial v}{\partial r}+\frac{v}{r}\frac{\partial v}{\partial \theta}+\frac{uv}{r}+w\frac{\partial v}{\partial z}\right)=-\frac{1}{r}\frac{\partial p}{\partial \theta}-2\rho\omega_z u+\rho\left(a_{gj,\theta}+a_{gg,\theta}\right)-\rho r\dot{\omega}_z$$

$$+\mu\left(\nabla^2 v-\frac{v}{r^2}+\frac{2}{r^2}\frac{\partial u}{\partial \theta}\right) \qquad (4\text{-}3)$$

$$\rho\left(\frac{\partial w}{\partial t}+u\frac{\partial w}{\partial r}+\frac{v}{r}\frac{\partial w}{\partial \theta}+w\frac{\partial w}{\partial z}\right)=-\frac{\partial p}{\partial z}+\rho\left(a_{gj,z}+a_{gg,z}\right)+\mu\nabla^2 w \qquad (4\text{-}4)$$

where

$$\nabla^2 = \frac{1}{r}\frac{\partial}{\partial r}\left(r\frac{\partial}{\partial r}\right) + \frac{1}{r^2}\frac{\partial^2}{\partial \theta^2} + \frac{\partial^2}{\partial z^2} \qquad (4\text{-}5)$$

In these formulations, $2\omega_z v$ and $2\omega_z u$ are the Coriolis acceleration, $r\omega_z^2$ is the centrifugal acceleration, and $r\dot{\omega}_z$ is the angular acceleration induced by the spinning motion of the spacecraft.

In the computation of fluid forces, moment, viscous stress and angular momentum acting on the container wall of the spacecraft, one has to consider those forces and moment in the inertia frame rather than the non-inertia frame, in particular for the case of the spinning motion in the z-axis. To show an example, one has to transform those vectors from the non-inertia frame to the inertia frame for the case of spinning motion in the z-axis.

$$\begin{bmatrix} F_x' \\ F_y' \\ F_z' \end{bmatrix} = \begin{bmatrix} \cos\omega_z t & -\sin\omega_z t & 0 \\ \sin\omega_z t & \cos\omega_z t & 0 \\ 0 & 0 & 1 \end{bmatrix} \begin{bmatrix} F_x \\ F_y \\ F_z \end{bmatrix} \qquad (4\text{-}6)$$

where prime symbol denotes vectors in the inertia frame while those parameters without the prime symbol indicate vectors in the non-inertia frame.

V. Initial and Boundary Conditions of Spacecraft Fluid System in Microgravity Environment

Governing equations of the fluid motion in on-orbit spacecraft fluid systems for non-inertia frame of spacecraft bound coordinates have been illustrated in Equations (4-1) to (4-6). These equations shall be combined with the characteristics of gravity gradient and gravity jitter accelerations as formulated in Equations (3-1) to (3-31). Initial and boundary conditions shall be introduced to accommodate solving fluid motion in on-orbit spacecraft fluid system for non-inertia frame coordinate (Hung et al., 1990 a,b,c; 1991 a,b,c,d,e,f,g,h,i,j).

Let the profile of the interface between gaseous and liquid fluids be given by:

$$\eta(t, r, \theta, z) = 0 \tag{5-1}$$

The initial condition of the profile of the interface between gaseous and liquid fluids at $t = t_o$ is assigned explicitly, and is given by:

$$\eta(t = t_o, r, \theta, z) = 0 \tag{5-2}$$

A set of boundary conditions has to be supplied for solving the equations. These initial interface profiles used in this study have been given explicitly through the steady state computations made by Hung and Leslie (1988) and Hung et al (1989 a,b,c,d) which were checked by the experiments carried out by Leslie (1985). These boundary conditions are as follows:

(1) Along the container wall, the following three boundary conditions apply:

(a) Interface between solid and liquid fluid: No-penetration and no-slip conditions assure that both the tangential and the normal components of the liquid velocity along the solid walls will vanish.

(b) Interface between solid and gaseous (vapor) fluid: Similar no-penetration and no-slip conditions as that shown for interface between solid and liquid fluid will apply.

(c) At the location of solid-liquid-gaseous (vapor) three phases interface: No-penetration, but not no-slip condition apply. This will assure that normal components of liquid and vapor velocities along the solid wall vanish, and allow a slipping flow of liquid and vapor fluids along the solid wall at three phase interface location. The velocity of slipping flow at this location is governed by the adhesive forces between fluids (liquid and gaseous) and solid walls.

Also, at this location of three phase interface, a constant contact angle is present in which the behaviors of wet or dry contacts are determined by Coulomb interaction between the fluids (liquid and vapor) and the surface phenomena (material and roughness) of solid walls.

(2) Along the interface between the liquid and gaseous fluids, the following two conditions apply:

(a) Kinematic surface boundary condition: The liquid (or gaseous) surface moves with the liquid (or gas) which implies

$$\frac{D\eta}{Dt}=0, or$$

$$\frac{\partial\eta}{\partial t}+u\frac{\partial\eta}{\partial r}+\frac{v}{r}\frac{\partial\eta}{\partial\theta}+w\frac{\partial\eta}{\partial z}=0 \qquad (5\text{-}3)$$

$$on\ \eta(t=t_\alpha, r, \theta, z)$$

(b) Interface stress condition: Across the liquid-vapor interface, the stress must be continuous. Based on Landu and Lifshitz (1959), the stress across the liquid-vapor interface can be expressed as

$$(P_G-P_L)n_i-[(\tau_{ij})_G-(\tau_{ij})_L]n_j=\sigma(\frac{1}{R_1}+\frac{1}{R_2})n_i \qquad (5\text{-}4)$$

where R_1 and R_2 are the radius of curvatures of two major axes at the point of interests on the surface of the liquid-vapor interface.

The expressions of radius of curvatures R_1 and R_2 in cylindrical coordinates from differential geometry can be shown as

$$\frac{1}{R_1}+\frac{1}{R_2}=\frac{EN-2FM+GL}{EG-F^2} \qquad (5\text{-}5)$$

where the relationship of cartesian and cylindrical coordinates for the curved

surface of liquid-vapor interface is

$$\begin{bmatrix} x \\ y \\ z \end{bmatrix} = \begin{bmatrix} r\cos\theta \\ r\sin\theta \\ H(t_\alpha, r, \theta) \end{bmatrix} \tag{5-6}$$

Here, the configuration of the liquid-vapor interface is $z = H\ (t = t_\alpha,\ r,\ \theta)$;

$$E = \left(\frac{\partial x}{\partial r}\right)^2 + \left(\frac{\partial y}{\partial r}\right)^2 + \left(\frac{\partial z}{\partial r}\right)^2 \tag{5-7}$$

$$F = \frac{\partial x}{\partial r}\frac{\partial x}{\partial \theta} + \frac{\partial y}{\partial r}\frac{\partial y}{\partial \theta} + \frac{\partial z}{\partial r}\frac{\partial z}{\partial \theta} \tag{5-8}$$

$$G = \left(\frac{\partial x}{\partial \theta}\right)^2 + \left(\frac{\partial y}{\partial \theta}\right)^2 + \left(\frac{\partial z}{\partial \theta}\right)^2$$

$$L = \frac{1}{(EG-F^2)^{\frac{1}{2}}}\begin{bmatrix} x''_{rr} & y''_{rr} & z''_{rr} \\ x'_r & y'_r & z'_r \\ x'_\theta & y'_\theta & z'_\theta \end{bmatrix} \tag{5-9}$$

$$M = \frac{1}{(EG-F^2)^{\frac{1}{2}}}\begin{bmatrix} x''_{r\theta} & y''_{r\theta} & z''_{r\theta} \\ x'_r & y'_r & z'_r \\ x'_\theta & y'_\theta & z'_\theta \end{bmatrix} \tag{5-10}$$

$$N = \frac{1}{(EG-F^2)^{\frac{1}{2}}}\begin{bmatrix} x''_{\theta\theta} & y''_{\theta\theta} & z''_{\theta\theta} \\ x'_r & y'_r & z'_r \\ x'_\theta & y'_\theta & z'_\theta \end{bmatrix} \tag{5-11}$$

where,

$$[x'_r, y'_r, z'_r] = \frac{\partial}{\partial r}[x, y, z,] \tag{5-12}$$

$$[x'_\theta, y'_\theta, z'_\theta] = \frac{\partial}{\partial \theta}[x, y, z] \tag{5-13}$$

and,

$$\begin{bmatrix} x''_{rr} & y''_{rr} & z''_{rr} \\ x''_{r\theta} & y''_{r\theta} & z''_{r\theta} \\ x''_{\theta\theta} & y''_{\theta\theta} & z''_{\theta\theta} \end{bmatrix} = \begin{bmatrix} \frac{\partial^2}{\partial r^2} \\ \frac{\partial^2}{\partial r \partial \theta} \\ \frac{\partial^2}{\partial \theta^2} \end{bmatrix} [x, y, z] \qquad (5\text{-}14)$$

Simplifying Equations (5-7) to (5-11), one obtains

$$EG-F^2 = r^2(1 + H_r^2 + \frac{1}{r^2}H_\theta^2) = r^2D^2$$

$$E = 1 + H_r^2, \; F = H_rH_\theta, \; G = r^2 + H_\theta^2$$

$$[H_r, H_\theta] = [\frac{\partial}{\partial r}, \frac{\partial}{\partial \theta}]H$$

$$D = (1 + H_r^2 + \frac{1}{r^2}H_\theta^2)^{\frac{1}{2}}$$

$$L = \frac{H_{rr}}{D}, \; M = \frac{(-H_\theta + rH_{r\theta})}{rD}, \; N = \frac{(r^2H_r + rH_{\theta\theta})}{rD}, \; \text{and}$$

Substituting these relations to Equation (5-4), the radius of the curvature on the curved surface of the configuration of liquid-vapor interface in cylindrical coordinates can be expressed as follows:

$$\frac{1}{R_1} + \frac{1}{R_2} = -\frac{1}{r}[\frac{\partial}{\partial r}(r\frac{H_r}{D}) + \frac{\partial}{\partial \theta}(\frac{H_\theta}{rD})] \qquad (5\text{-}15)$$

Here, in Equations (5-4) and (5-15)

$$\tau_{ij} = \mu(\frac{\partial u_i}{\partial x_j} + \frac{\partial u_j}{\partial x_i} + \frac{2}{3}\frac{\partial u_k}{\partial x_k}\delta_{ij}) + \zeta\frac{\partial u_k}{\partial x_k}\delta_{ij}$$

is the viscous stress tensor; μ, the viscous coefficient of the first kind; ζ,

the viscous coefficient of the second kind; P, the pressure; σ, the surface tension of the liquid-vapor interface; and n_j, the unit vector normal to the interface; and δ_{ij}, the Kronecker's delta function. Also, subscripts G and L denote conditions at gaseous and liquids fluids, respectively, across the liquid-vapor interface.

The fluid stresses across the liquid-vapor interface can be decomposed to the components normal (n_i, a unit vector) and tangential (t_i, a unit vector) to the interface. For the component tangential to the interface, one can take a dot product of a unit vector tangential to the interface, t_i, to Equations (5-4) and (5-15), which leads to

$$[(\tau_{ij} t_i n_j)]_L = [(\tau_{ij} t_i n_j)]_G \qquad (5\text{-}16)$$

since $n_i t_i = 0$.

For the component normal to the interface, one can also take a dot product of a unit vector normal to the interface, n_i, to Equations (5-4) and (5-15), which leads to

$$P_G - P_L - [(\tau_{ij} n_i n_j)_G - (\tau_{ij} n_i n_j)_L] = -\frac{\sigma}{r}\left[\frac{\partial}{\partial r}\left(\frac{rH_r}{D}\right) + \frac{\partial}{\partial \theta}\left(\frac{H_\theta}{rD}\right)\right]$$

For components normal to the interface along the (r, θ, z) directions in cylindrical coordinates can be obtained by taking dot products of n_r, n_θ, n_z separately to Equations (5-4) and (5-15), which are expressed as

$$(P_G - P_L)\begin{bmatrix} n_r \\ n_\theta \\ n_z \end{bmatrix} - \begin{bmatrix} (\tau_{rj} n_j)_G - (\tau_{rj} n_j)_L \\ (\tau_{\theta j} n_j)_G - (\tau_{\theta j} n_j)_L \\ (\tau_{zj} n_j)_G - (\tau_{zj} n_j)_L \end{bmatrix}$$

where (n_r, n_θ, n_z) is the unit vector normal to the interface in cylindrical coordinates (r, θ, z).

$$= -\frac{\sigma}{r}\left[\frac{\partial}{\partial r}\left(\frac{rH_r}{D}\right) + \frac{\partial}{\partial\theta}\left(\frac{H_\theta}{rD}\right)\right]\begin{bmatrix} n_r \\ n_\theta \\ n_z \end{bmatrix} \qquad (5\text{-}18)$$

For a special case of axial symmetry, component normal to the interface, shown in Equation (5-17), can be simplified and becomes

$$P_G - P_L - (\tau_{ij}n_i n_j)_G + (\tau_{ij}n_i n_j)_L$$

$$= -\frac{\sigma}{r}\frac{d}{dr}\left[\frac{r\phi}{(1+\phi^2)^{\frac{1}{2}}}\right] \qquad (5\text{-}19)$$

since $\partial/\partial\theta = 0$, $H_r = \partial H/\partial r = dz/dr = \phi$, $H_\theta = 0$ and $D = (1+\phi^2)^{1/2}$ for the case of axial symmetry.

VI. Characteristics of Slosh Wave Induced Fluctuations in Fluid Moment and Angular Momentum

Slosh wave induced fluctuations in the fluid system of the rotating dewar introduce time-dependent disturbances in moment and angular momentum of spacecraft fluid system. In this study, there are induced angular velocities along the yawing, pitching and rolling axes due to the fluid motion inside rotating container. These angular velocities in yawing, pitching and rolling axes, caused by the fluid flows in a partially liquid-filled container, readjust the angular velocity in rolling axis.

In order to accommodate the spacecraft dynamics of yawing, pitching and rolling, cylindrical coordinates (shown in Figure 1) of rotating container is transformed into cartesian coordinates based on $(x, y, z) = (r\cos\theta, r\sin i\theta, z)$ with corresponding velocity components $(V_x, V_y, V_z) = (u\cos\theta - v\sin\theta, u\sin\theta + v\cos\theta, w)$. If spacecraft is rotated with respect to mass center at (r_c, θ_c, z_c) in cylindrical coordinates, location of mass center in cartesian coordinates becomes $(x_c, y_c, z_c) = (r_c\cos\theta_c, r_c\sin\theta_c, z_c)$. Induced angular velocities $(\bar{\omega}_x, \bar{\omega}_y,$

$\tilde{\omega}_z$) in cartesian coordinates becomes

$$\begin{bmatrix}\tilde{\omega}_x\\ \tilde{\omega}_y\\ \tilde{\omega}_z\end{bmatrix}=\begin{bmatrix}K_{xx} & -K_{xy} & K_{xz}\\ K_{yx} & K_{yy} & -K_{yz}\\ -K_{zx} & K_{zy} & K_{zz}\end{bmatrix}\begin{bmatrix}V_x\\ V_y\\ V_z\end{bmatrix} \qquad (6\text{-}1)$$

where

$$K_{xx}=K_{yy}=K_{zz}=0$$

$$\begin{bmatrix}K_{xy}\\ K_{yx}\end{bmatrix}= (z-z_c)\begin{bmatrix}[(y-y_c)^2+(z-z_c)^2]^{-1}\\ [(x-x_c)^2+(z-z_c)^2]^{-1}\end{bmatrix}$$

$$\begin{bmatrix}K_{xz}\\ K_{zx}\end{bmatrix}= (y-y_c)\begin{bmatrix}[(y-y_c)^2+(z-z_c)^2]^{-1}\\ [(x-x_c)^2+(y-y_c)^2]^{-1}\end{bmatrix}$$

$$\begin{bmatrix}K_{yz}\\ K_{zy}\end{bmatrix}= (x-x_c)\begin{bmatrix}[(x-x_c)^2+(z-z_c)^2]^{-1}\\ [(x-x_c)^2+(y-y_c)^2]^{-1}\end{bmatrix}$$

As the velocity components are given by

$$\begin{bmatrix}V_x\\ V_y\\ V_z\end{bmatrix}=\begin{bmatrix}\cos\theta & -\sin\theta & 0\\ \sin\theta & \cos\theta & 0\\ 0 & 0 & 1\end{bmatrix}\begin{bmatrix}u\\ v\\ w\end{bmatrix}, \qquad (6\text{-}2)$$

the relationship between the components of induced angular velocity and flow velocity in cylindrical coordinates can be expressed in the following formulation:

$$\begin{bmatrix}\tilde{\omega}_x\\ \tilde{\omega}_y\\ \tilde{\omega}_z\end{bmatrix}=\begin{bmatrix}\tilde{K}_{xx} & \tilde{K}_{xy} & \tilde{K}_{xz}\\ \tilde{K}_{yx} & \tilde{K}_{yy} & \tilde{K}_{yz}\\ \tilde{K}_{zx} & \tilde{K}_{zy} & \tilde{K}_{zz}\end{bmatrix}\begin{bmatrix}u\\ v\\ w\end{bmatrix} \qquad (6\text{-}3)$$

where

$$\begin{bmatrix}\tilde{K}_{xx}\\ \tilde{K}_{xy}\\ \tilde{K}_{xz}\end{bmatrix}=\begin{bmatrix}-(z-z_c)\sin\theta\\ -(z-z_c)\cos\theta\\ r\sin\theta-r_c\sin\theta_c\end{bmatrix}\left[(r\sin\theta-r_c\sin\theta_c)^2+(z-z_c)^2\right]^{-1}$$

$$\begin{bmatrix}\tilde{K}_{yx}\\ \tilde{K}_{yy}\\ \tilde{K}_{yz}\end{bmatrix}=\begin{bmatrix}(z-z_c)\cos\theta\\ -(z-z_c)\sin\theta\\ -(r\cos\theta-r_c\cos\theta_c)\end{bmatrix}\left[(r\cos\theta-r_c\cos\theta_c)^2+(z-z_c)^2\right]^{-1}$$

$$\begin{bmatrix}\tilde{K}_{zx}\\ \tilde{K}_{zy}\\ \tilde{K}_{zz}\end{bmatrix}=\begin{bmatrix}-r_c\sin(\theta-\theta_c)\\ r-r_c\cos(\theta-\theta_c)\\ 0\end{bmatrix}\left[r^2+r_c^2-2rr_c\cos(\theta-\theta_c)\right]^{-1}$$

For the case of the GP-B, the axis of rotation is always fixed at the point of proof mass which is located at the geometric center of the dewar at (x_c, y_c, z_c = (0, 0, L_c) where L_c = 1/2 L and L is the height of the dewar (see Figure 1). By using the computed results of induced angular velocity shown in Equation (6-3), one can compute the angular momentum (H_x, H_y, H_z) as follows:

$$\begin{bmatrix}H_x\\ H_y\\ H_z\end{bmatrix}=\rho_v\left\{\iiint\begin{bmatrix}\tilde{I}_{xx} & -\tilde{I}_{xy} & -\tilde{I}_{xz}\\ -\tilde{I}_{yx} & \tilde{I}_{yy} & -\tilde{I}_{yz}\\ -\tilde{I}_{zx} & -\tilde{I}_{zy} & \tilde{I}_{zz}\end{bmatrix}\begin{bmatrix}\tilde{\omega}_x\\ \tilde{\omega}_y\\ \tilde{\omega}_z\end{bmatrix}+\begin{bmatrix}r\sin\theta v_{c,z} & -(z-L_c)v_{c,y}\\ (z-L_c)v_{c,x} & -r\cos\theta v_{c,z}\\ r\cos\theta v_{c,y} & -r\sin\theta v_{c,x}\end{bmatrix}\right\}_{vapor} r\,d\theta\,dr\,dz$$

$$+\rho_L\left\{\iiint\begin{bmatrix}\tilde{I}_{xx} & -\tilde{I}_{xy} & -\tilde{I}_{xz}\\ -\tilde{I}_{yx} & \tilde{I}_{yy} & -\tilde{I}_{yz}\\ -\tilde{I}_{zx} & -\tilde{I}_{zy} & \tilde{I}_{zz}\end{bmatrix}\begin{bmatrix}\tilde{\omega}_x\\ \tilde{\omega}_y\\ \tilde{\omega}_z\end{bmatrix}+\begin{bmatrix}r\sin\theta v_{c,z} & -(z-L_c)v_{c,y}\\ (z-L_c)v_{c,x} & -r\cos\theta v_{c,z}\\ r\cos\theta v_{c,y} & -r\sin\theta v_{c,x}\end{bmatrix}\right\}_{liquid} r\,d\theta\,dr\,dz \qquad (6\text{-}4)$$

where

$\tilde{I}_{xx} = r^2\sin^2\theta + (z - L_c)^2$; $\tilde{I}_{xy} = \tilde{I}_{yx} = r^2\sin\theta\cos\theta$

$\tilde{I}_{yy} = r^2\cos^2\theta + (z - L_c)^2$; $\tilde{I}_{xz} = \tilde{I}_{zx} = r(z - L_c)\cos\theta$

$\tilde{I}_{zz} = r^2$; $\tilde{I}_{yz} = \tilde{I}_{zy} = r(z - L_c)\sin\theta$

and

$$\begin{bmatrix} V_{c,x} \\ V_{c,y} \\ V_{c,z} \end{bmatrix} = \begin{bmatrix} \cos\theta & -\sin\theta & 0 \\ \sin\theta & \cos\theta & 0 \\ 0 & 0 & 1 \end{bmatrix} \begin{bmatrix} u_c \\ v_c \\ w_c \end{bmatrix}$$

The moment of spacecraft can be computed from the time rate of change of the angular momentum, i.e.,

$$\begin{bmatrix} M_x \\ M_y \\ M_z \end{bmatrix} = \frac{d}{dt} \begin{bmatrix} H_x \\ H_y \\ H_z \end{bmatrix} + \begin{bmatrix} \omega_y H_z & -\omega_z H_y \\ \omega_z H_x & -\omega_x H_y \\ \omega_x H_y & -\omega_y H_x \end{bmatrix} \tag{6-5}$$

where $\omega_i = (\omega_x, \omega_y, \omega_z)$ denotes pitching, yawing and rolling angular velocities of spacecraft in inertia frame.

VII. Mathematical Formulation of Fluid Stresses and Moment Fluctuations Due to Slosh Waves

For the purpose of considering large amplitude slosh wave activated fluid stresses exerted on the solid walls of the dewar, the fluid stresses are decomposed into the tangential and normal components to the walls which can be expresses as follows:

$$\Pi_t = \mu \left(\frac{\partial u_\alpha}{\partial x_\beta} + \frac{\partial u_\beta}{\partial x_\alpha} \right) \hat{t}_\alpha \hat{n}_\beta \tag{7-1}$$

$$\Pi_n = P\delta_{\alpha\beta} - \mu \left(\frac{\partial u_\alpha}{\partial x_\beta} + \frac{\partial u_\beta}{\partial x_\alpha} \right) \hat{n}_\alpha \hat{n}_\beta \tag{7-2}$$

where Π_t denotes the tangential component of fluid stresses; Π_n, the normal component of fluid stresses; P, the thermodynamic pressure; u_α, fluid velocity in α direction; $\hat{t}_\alpha$, unit vector tangential to the wall; $\hat{n}_\beta$, unit vector normal to the wall; μ, the molecular viscosity coefficient of fluid; and $\delta_{\alpha\beta}$, the Dirac

delta function. Subscripts α and β imply the directions of flow fields.

Figures 2(A) and 2(B) show the geometry of GP-B dewar propellant tank in both r-z and r-θ planes, respectively. In order to make the computation of fluid stresses match the geometry of the dewar tank, mathematical formulations have been divided into three sections: (A) Top wall (dome) section, (B) Bottom wall (dome) section, (C) Cylindrical section (including probe section of the inner wall of dewar) and (D) Baffle plates section. There are several plates of baffle inserted in the dewar [see Figure 3(A) and 3(B) for baffle board illustration]. Baffles with the shape of hollow circular plate with an inner radius R_1, and an outer radius R_2 are installed along the probe column of the dewar located at z = L_i, where i = 1, 2, ..., n plates and the thickness of each plate is d. Figure 4 shows the GP-B dewar container equipped with probe and baffle boards.

(A) Top Wall (Dome) Section:

$$(\Pi_t)^{r-z}_{Top\ Wall}=\mu\left(\frac{\partial u}{\partial z}+\frac{\partial w}{\partial r}\right)\cos 2\phi \tag{7-3}$$

$$(\Pi_t)^{r-\theta}_{Top\ Wall}=\mu\left[\left(\frac{1}{r}\frac{\partial u}{\partial \theta}+\frac{\partial v}{\partial r}\right)\cos\phi+\left(\frac{1}{r}\frac{\partial w}{\partial \theta}+\frac{\partial v}{\partial z}\right)\sin\phi\right] \tag{7-4}$$

$$(\Pi_n)_{Top\ Wall}=P+\mu\left(\frac{\partial u}{\partial z}+\frac{\partial w}{\partial r}\right)\sin 2\phi \tag{7-5}$$

(B) Bottom Wall (Dome) Section:

$$(\Pi_t)^{r-z}_{Bottom\ Wall}=\mu\left(\frac{\partial u}{\partial z}+\frac{\partial w}{\partial r}\right)\cos 2\phi \tag{7-6}$$

$$(\Pi_t)^{r-\theta}_{Bottom\ Wall}=\mu\left[\left(\frac{1}{r}\frac{\partial u}{\partial \theta}+\frac{\partial v}{\partial r}\right)\cos\phi-\left(\frac{1}{r}\frac{\partial w}{\partial \theta}+\frac{\partial v}{\partial z}\right)\sin\phi\right] \tag{7-7}$$

$$(\Pi_n)_{Bottom\ Wall}=P-\mu\left(\frac{\partial u}{\partial z}+\frac{\partial w}{\partial r}\right)\sin 2\phi \tag{7-8}$$

(C) Cylindrical Section (including probe section of the inner wall of dewar):

$$(\Pi_t)^{r-z}_{Cylindrical}=\mu\left(\frac{\partial u}{\partial z}+\frac{\partial w}{\partial r}\right) \tag{7-9}$$

$$(\Pi_t)^{r-\theta}_{Cylindrical}=\mu\left(\frac{1}{r}\frac{\partial u}{\partial \theta}+\frac{\partial v}{\partial r}\right) \tag{7-10}$$

$$(\Pi_n)_{Cylindrical}=P \tag{7-11}$$

(D) Baffle Plates Section:

$$(\Pi_t)^{r-z}_{Baffle} = \mu\left(\frac{\partial u}{\partial z} + \frac{\partial w}{\partial r}\right) \tag{7-12}$$

$$(\Pi_t)^{r-\theta}_{Baffle} = \mu\left(\frac{1}{r}\frac{\partial u}{\partial \theta} + \frac{\partial v}{\partial r}\right) \tag{7-13}$$

$$(\Pi_n)_{Baffle} = \pm P \tag{7-14}$$

where ϕ is the azimuth angle of the dome; and $(\Pi_t)^{r-z}$ and $(\Pi_t)^{r-\theta}$ denote tangential stresses in r-z and r-θ planes of the dewar, respectively. Velocity components in cylindrical coordinates of (r, θ, z) are shown as (u, v, w).

The stress distribution shown in Eqs. (7-3) to (7-14) can be integrated with respect to area and obtain the tangential and normal forces on top wall, bottom wall, and cylindrical sections of the dewar.

(A) Top Wall (Dome) Sections:

$$\begin{bmatrix}(F_t)^{r-z}\\(F_t)^{r-\theta}\\(F_n)\end{bmatrix}_{Top\ Wall}=\iint\begin{bmatrix}(\Pi_t)^{r-z}\\(\Pi_t)^{r-\theta}\\(\Pi_n)\end{bmatrix}_{Top\ Wall}R_d^2\cos\phi\, d\phi\, d\theta \tag{7-15}$$

(B) Bottom Wall (Dome) Section:

$$\begin{bmatrix} (F_t)^{r-z} \\ (F_t)^{r-\theta} \\ (F_n) \end{bmatrix}_{Bottom\ Wall} = \iint \begin{bmatrix} (\Pi_t)^{r-z} \\ (\Pi_t)^{r-\theta} \\ (\Pi_n) \end{bmatrix}_{Bottom\ Wall} R_d^2 \cos\phi d\phi d\theta \qquad (7\text{-}16)$$

(C) Cylindrical Section (including probe section of the inner wall of dewar):

$$\begin{bmatrix} (F_t)^{r-z} \\ (F_t)^{r-\theta} \\ (F_n) \end{bmatrix}_{Cylindrical} = \iint \begin{bmatrix} (\Pi_t)^{r-z} \\ (\Pi_t)^{r-\theta} \\ (\Pi_n) \end{bmatrix}_{Inner\ Cylinder} R_{c1} d\theta dz$$

$$+ \iint \begin{bmatrix} (\Pi_t)^{r-z} \\ (\Pi_t)^{r-\theta} \\ (\Pi_n) \end{bmatrix}_{Outer\ Cylinder} R_{c2} d\theta dz \qquad (7\text{-}17)$$

(D) Baffle Plate Section:

$$\begin{bmatrix} (F_t)^{r-\theta} \\ (F_t)^{r-\theta} \\ (F_n) \end{bmatrix}_{Baffle} = \iint \begin{bmatrix} (\Pi_t)^{r-z} \\ (\Pi_t)^{r-\theta} \\ (\Pi_n) \end{bmatrix}_{Baffle} r dr d\theta \qquad (7\text{-}18)$$

where R_d and ϕ denote the radius and the azimuth angle of the dome section, respectively; and R_{c1} and R_{c2} are the radii of the inner and outer walls of the cylindrical section of the dewar (see Figs. 2 and 3).

In order to accommodate the spacecraft dynamics of pitching, yawing and rolling, cylindrical coordinates (shown in Figs. 2 and 3) of the rotating container is transformed into cartesian coordinates based on $(x, y, z) = (r\cos\theta, r\sin\theta, z)$ with corresponding velocity components $(v_x, v_y, v_z) = (u\cos\theta - v\sin\theta, u\sin\theta + v\cos\theta, w)$. For the case of the GP-B Spacecraft, the axis of rotation is always fixed at the point of proof mass which is located at the geometrical center of the dewar at $(x_c, y_c, z_c) = (0, 0, L/2)$, where L is the height of the dewar (see Figs. 2 and 3). To fulfill this goal, stress distributions, shown in

Eqs. (7-15) to (7-18), have to be recalculated in the (x, y, z) directions (see Figs. 2 and 3).

$$F_x=\left\{\left[\iint-(\Pi_t)^{r-z}_{Top\ Wall}+\iint(\Pi_t)^{r-z}_{Bottom\ Wall}\right]R_d^2\cos\phi\cdot\sin\phi\cdot\cos\theta\,d\phi\,d\theta\right\}$$

$$+\left\{\left[\iint-(\Pi_t)^{r-\theta}_{Top\ Wall}-\iint(\Pi_t)^{r-\theta}_{Bottom\ Wall}\right]R_d^2\cos\phi\cdot\sin\theta\,d\phi\,d\theta\right\}$$

$$+\left\{\left[\iint(\Pi_n)_{Top\ Wall}+\iint(\Pi_n)_{Bottom\ Wall}\right]R_d^2\cos^2\phi\cdot\cos\theta\,d\phi\,d\theta\right\}$$

$$+\left\{\left[\iint-(\Pi_t)^{r-\theta}_{InnerCylinder}\sin\theta+\iint(\Pi_n)_{InnerCylinder}\cos\theta\right]R_{c1}\,d\theta\,dz\right\}$$

$$+\sum_i\left\{\left[\iint(\Pi_t)^{r-z}_{Baffle}\cos\theta\,r\,dr\,d\theta+\iint(\Pi_t)^{r-\theta}_{Baffle}\sin\theta\,r\,dr\,d\theta\right]_{z=L_1-\frac{d}{2}}\right\}$$

$$+\sum_i\left\{\left[\iint(\Pi_t)^{r-z}_{Baffle}\cos\theta\,r\,dr\,d\theta+(\Pi_t)^{r-\theta}_{Baffle}\sin\theta\,r\,dr\,d\theta\right]_{z=L_1+\frac{d}{2}}\right\} \qquad (7\text{-}19)$$

$$F_y=\left\{\left[\iint-(\Pi_t)^{r-z}_{Top\ Wall}+\iint(\Pi_t)^{r-z}_{Bottom\ Wall}\right]R_d^2\cos\phi\cdot\sin\phi\cdot\sin\theta\,d\phi\,d\theta\right\}$$

$$+\left\{\left[\iint-(\Pi_t)^{r-\theta}_{Outer\ Cylinder}\sin\theta+\iint(\Pi_n)_{Outer\ Cylinder}\cos\theta\right]R_{c2}\,d\theta\,dz\right\}$$

$$+\left\{\left[\iint(\Pi_t)^{r-\theta}_{Top\ Wall}+\iint(\Pi_t)^{r-\theta}_{Bottom\ Wall}\right]R_d^2\cos\phi\cdot\cos\theta\,d\phi\,d\theta\right\}$$

$$+\left\{\left[\iint(\Pi_n)_{Top\ Wall}+\iint(\Pi_n)_{Bottom\ Wall}\right]R_d^2\cos^2\phi\cdot\sin\theta\,d\phi\,d\theta\right\}$$

$$+\left\{\left[\iint(\Pi_t)^{r-\theta}_{InnerCylinder}\cos\theta+\iint(\Pi_n)_{InnerCylinder}\sin\theta\right]R_{c1}\,d\theta\,dz\right\}$$

$$+\left\{\left[\iint(\Pi_n)_{Outer\ Cylinder}\cos\theta+\iint(\Pi_n)_{Outer\ Cylinder}\sin\theta\right]R_{c1}d\theta dz\right\}$$

$$+\sum_i\left\{\left[\iint(\Pi_t)^{r-z}_{Baffle}\sin\theta r dr d\theta+(\Pi_t)^{r-\theta}_{Baffle}\cos\theta r dr d\theta\right]_{z=L_i-\frac{d}{2}}\right\}$$

$$+\sum_i\left\{\left[\iint(\Pi_t)^{r-z}_{Baffle}\sin\theta r dr d\theta+\iint(\Pi_t)^{r-\theta}_{Baffle}\cos\theta r dr d\theta\right]_{z=L_i+\frac{d}{2}}\right\} \qquad (7\text{-}20)$$

$$F_z=\left\{\left[\iint(\Pi_t)^{r-z}_{Top\ Wall}+\iint(\Pi_t)^{r-z}_{Bottom\ Wall}\right]R_d^2\cos^2\phi d\phi d\theta\right\}+\left\{\left[\iint(\Pi_n)_{Top\ Wall}\right.\right.$$

$$\left.\left.+\iint(\Pi_n)_{Bottom\ Wall}\right]R_d^2\cos\phi\cdot\sin\phi d\phi d\theta\right\}+\left[\iint(\Pi_t)^{r-z}_{InnerCylinder}R_{c1}d\theta dz+\iint(\Pi_t)^{r-z}_{OuterCylinder}R_{c2}d\theta dz\right] \qquad (7\text{-}21)$$

The moment of stress force acting on the dewar wall of the container can be computed from the cross product of moment arm, [which is the perpendicular distance from the location of proof mass of the spacecraft to the total forces], and the total forces. Components of the moment can be computed from the following formulations:

$$M_x=\left[\iint(\Pi_t)^{r-z}_{Top\ Wall}+\iint(\Pi_t)^{r-z}_{Bottom\ Wall}\right]R_d^3\cos^3\phi\cdot\sin\theta d\phi d\theta$$

$$+\left[\iint(\Pi_n)_{Top\ Wall}+\iint(\Pi_n)_{Bottom\ Wall}\right]R_d^3\cos^2\phi\cdot\sin\phi\cdot\sin\theta d\phi d\theta$$

$$+\left\{\left[\iint-(\Pi_n)^{r-\theta}_{Outer\ Cylinder}\sin\theta+\iint(\Pi_n)_{Outer\ Cylinder}\cos\theta\right]R_{c2}d\theta dz\right\}$$

$$+\left[\iint(\Pi_t)^{r-z}_{Inner\ Cylinder}R_{c1}^2\sin\theta d\theta dz+\iint(\Pi_t)^{r-z}_{Outer\ Cylinder}R_{c2}^2\sin\theta d\theta dz\right]+\left\{\left[\iint-(\Pi_t)^{r-z}_{Top\ Wall}+\iint(\Pi_t)^{r-z}_{Bottom\ Wall}\right]\right.$$

$$\left.\cdot(L_c-L_d+R_d\sin\phi)R_d^2\cos\phi\cdot\sin\phi\cdot\sin\theta d\phi d\theta\right\}+\left[\iint(\Pi_t)^{r-\theta}_{Top\ Wall}\right.$$

$$+\iint (\Pi_t)^{r-\theta}_{Bottom\ Wall}](L_c-L_d+R_d\sin\phi)R_d^2\cos\phi\cdot\cos\theta d\phi d\theta+[\iint (\Pi_n)_{Top\ Wall}$$

$$+\iint (\Pi_n)_{Bottom\ Wall}]\ (L_c-L_d+R_d\sin\psi)\ R_d{}^2\cos^2\psi\cdot\sin\theta d\psi d\theta$$

$$+\{\Big[\iint (\Pi_t)^{r-\theta}_{Inner\ Cylinder}\cos\theta+\iint (\Pi_n)_{Inner\ Cylinder}\sin\theta\Big](z-L_c)R_{c1}d\theta dz$$

$$+\Big[\iint (\Pi_t)^{r-\theta}_{Outer\ Cylinder}\cos\theta+\iint (\Pi_n)_{Outer\ Cylinder}\sin\theta\Big]\ (z-L_c)\ R_{c2}d\theta dz\}$$

$$+\sum_i \left\{\left[-\iint (\Pi_t)^{r-z}_{Baffle}\sin\theta r dr d\theta+\iint (\Pi_t)^{r-\theta}_{Baffle}\cos\theta r dr d\theta\right]_{z=L_i-\frac{d}{2}}(-L_c+L_i-\frac{d}{2})\right\}$$

$$+\sum_i \left\{\left[-\iint (\Pi_t)^{r-z}_{Baffle}\sin\theta r dr d\theta+\iint (\Pi_t)^{r-\theta}_{Baffle}\cos\theta r dr d\theta\right]_{z=L_i+\frac{d}{2}}(-L_c+L_i+\frac{d}{2})\right\} \quad (7-22)$$

$$M_y=\Big[\iint (\Pi_t)^{r-z}_{Top\ Wall}+\iint (\Pi_t)^{r-z}_{Bottom\ Wall}\Big](L_c-L_d+R_d\sin\phi)R_d^2\cos\phi\cdot\sin\phi\cdot\cos\theta d\phi d\theta$$

$$+\Big[\iint -(\Pi_t)^{r-\theta}_{Top\ Wall}-\iint (\Pi_t)^{r-\theta}_{Bottom\ Wall}\Big]\ (L_c-L_d+R_d\sin\phi)\cdot R_d^2\cos\phi\cdot\sin\theta d\phi d\theta$$

$$+\Big[\iint (\Pi_n)_{Top\ Wall}+\iint (\Pi_n)_{Bottom\ Wall}\Big]\ (L_c-L_d+R_d\sin\phi)\ R_d^2\cdot\cos^2\phi\cdot\cos\theta d\phi d\theta$$

$$+\{\Big[\iint -(\Pi_t)^{r-\theta}_{Inner\ Cylinder}\sin\theta+\iint (\Pi_n)_{Inner\ Cylinder}\cdot\cos\theta\Big]\cdot(z-L_c)R_{c1}d\theta dz$$

$$+\Big[\iint -(\Pi_t)^{r-\theta}_{Outer\ Cylinder}\sin\theta+\iint (\Pi_n)_{Outer\ Cylinder}\cos\theta\Big]\ (z-L_c)\ R_{c2}d\theta dz\}$$

$$-\{[\iint (\Pi_t)^{r-z}_{Top\ Wall}+\iint (\Pi_t)^{r-z}_{Bottom\ Wall}]\cdot R_d^3\cos^2\phi\cdot\cos\theta d\phi d\theta+[\iint (\Pi_n)_{Top\ Wall}$$

$$+\iint (\Pi_n)_{BottomWall}]\cdot R_d^3\cdot\cos^2\phi\cdot\sin\phi\cdot\cos\theta d\phi d\theta$$

$$+\iint (\Pi_t)^{r-z}_{Inner\ Cylinder}R_{c1}^2\cos\phi d\phi d\theta+\iint (\Pi_t)^{r-z}_{Outer\ Cylinder}R_{c2}^2\cos\phi d\phi d\theta\}$$

$$+\sum_i \left\{ \left[\iint (\Pi_t)^{r-z}_{Baffle} \cos\theta r dr d\theta + \iint (\Pi_t)^{r-\theta}_{Baffle} \sin\theta r dr d\theta \right]_{z=L_1-\frac{d}{2}} (-L_c+L_1-\frac{d}{2}) \right\}$$

$$+\sum_i \left\{ \left[-\iint (\Pi_t)^{r-z}_{Baffle} \cos\theta r dr d\theta + \iint (\Pi_t)^{r-\theta}_{Baffle} \sin\theta r dr d\theta \right]_{z=L_1+\frac{d}{2}} (-L_c+L_1+\frac{d}{2}) \right\} \qquad (7\text{-}23)$$

$$M_z = \left[\iint -(\Pi_t)^{r-z}_{Top\ Wall} + \iint (\Pi_t)^{r-z}_{Bottom\ Wall} \right] R_d^3 \cos^2\phi \cdot \sin\phi \cdot \sin\theta \cdot \cos\theta d\phi d\theta$$

$$+ \left[\iint (\Pi_t)^{r-\theta}_{Top\ Wall} + \iint (\Pi_t)^{r-\theta}_{Bottom\ Wall} \right] R_d^3 \cos^2\phi \cdot \cos^2\theta d\phi d\theta$$

$$+ \left[\iint (\Pi_n)_{Top\ Wall} + \iint (\Pi_n)_{Bottom\ Wall} \right] R_d^3 \cos^3\phi \cdot \sin\theta \cdot \cos\theta d\phi d\theta$$

$$+ \left[\iint (\Pi_t)^{r-\theta}_{Inner\ Cylinder} \cos\theta + \iint (\Pi_n)_{Inner\ Cylinder} \cdot \sin\theta \right] R_{c1}^2 \cos\theta d\theta dz$$

$$\{ + \left[\iint (\Pi_t)^{r-\theta}_{Outer\ Cylinder} \cos\theta + \iint (\Pi_n)_{Outer\ Cylinder} \sin\theta \right] R_{c2}^2 \cos\theta d\theta dz$$

$$- \{ \left[\iint -(\Pi_t)^{r-z}_{Top\ Wall} + \iint (\Pi_t)^{r-z}_{Bottom\ Wall} \right] \cdot R_d^3 \cos^2\phi \cdot \sin\phi \cdot \cos\theta \cdot \sin\theta d\phi d\theta$$

$$+ \left[\iint -(\Pi_t)^{r-\theta}_{Top\ Wall} - \iint (\Pi_t)^{r-\theta}_{Bottom\ Wall} \right] R_d^3 \cos^2\phi \cdot \sin^2\theta d\phi d\theta$$

$$+ \left[\iint (\Pi_n)_{Top\ Wall} + (\Pi_n)_{Bottom\ Wall} \right] R_d^3 \cos^3\phi \cdot \cos\theta \cdot \sin\theta d\phi d\theta$$

$$+ \left[\iint -(\Pi_t)^{r-\theta}_{Inner\ Cylinder} \sin\theta + \iint (\Pi_n)_{Inner\ Cylinder} \cos\theta \right] R_{c1}^2 \sin\theta d\theta dz$$

$$+ \left[\iint -(\Pi_t)^{r-\theta}_{Outer\ Cylinder} \sin\theta + \iint (\Pi_n)_{Outer\ Cylinder} \cos\theta \right] R_{c2} \sin\theta d\theta dz \} \qquad (7\text{-}24)$$

where L_d denotes the height of the dome (see Fig. 2).

After the integration of Eqs. (7-19) thru (7-24), components of the moment can be rewritten as the following expression:

$$\begin{bmatrix} M_x \\ M_y \\ M_z \end{bmatrix} = \begin{bmatrix} L_y F_z - (L_z - L_c) F_y \\ (L_z - L_c) F_x - L_x F_z \\ L_x F_y - L_y F_x \end{bmatrix} \qquad (7\text{-}25)$$

where L_x, L_y, and L_z denote the components of the moment arm along x, y, and z axes, respectively.

By using the relation of $F_\alpha L_\alpha = 0$, or $F_x L_x + F_y L_y + F_z (L_z - L_c) = 0$, moment arms of the moment of fluid stress moment induced by the slosh wave excitation can be computed from the following relations:

$$\begin{bmatrix} L_x \\ L_y \\ L_z - L_c \end{bmatrix} = \frac{1}{F_x^2 + F_y^2 + F_z^2} \begin{bmatrix} F_y M_z - F_z M_y \\ F_z M_x - F_x M_z \\ F_x M_y - F_y M_x \end{bmatrix} \qquad (7\text{-}26)$$

VIII. Methods of Numerical Simulation

Detailed descriptions of the computational algorithm applicable to cryogenic fluid management under microgravity are also given in our earlier studies (Hung et al., 1990 a,b,c). In this report, a full-scale GP-B and AXAF spacecraft propellant dewar tanks with a radius of 68 cm and a height of 145 cm will be used in the numerical simulation. The propellant tank is 80% filled with cryogenic liquid helium for the GP-B dewar while the rest of the ullage is filled with helium vapor. The temperature of cryogenic helium is 1.8 K. In this study the following data were used: liquid helium density = 0.146 g/cm^3, helium vapor density = 0.00147 g/cm^3, fluid pressure = 1.66 x 10^3 dyne/cm^2, surface tension coefficient at the interface between liquid helium and helium vapor = 0.353 dyne/cm, liquid helium viscosity coefficient = 9.61 x 10^{-5} cm^2/s; and contact angle = 5°. The initial profiles of the liquid-vapor interface for the rotating dewar are determined from computations based on algorithms developed for the steady state formulation of microgravity fluid management (Hung et al., 1990 a,b,c).

A staggered grid for the velocity components is used in this computer program. The method was developed by Harlow and Welch (1965) for their MAC (marker-and-cell) method of studying fluid flows along a free surface. The

finite difference method employed in this numerical study was the "Hybrid Scheme" developed by Spalding (1972). The formulation for this method is valid for any arbitrary interface location between the grid points and is not limited to middle point interfaces (Patankar and Spalding, 1972). An algorithm for a semi-implicit method (Patankar, 1980) was used as the procedure for modeling the flow field. The time step is determined automatically based on the size of the grid points and the velocity of flow fields. A detailed description of the computational algorithm applicable to microgravity fluid management is illustrated in our earlier studies (Hung et al., 1990 a,b,c). Figures 5(A) and 5(B) show the distribution of grid points for the dewar tank with probe for GP-B dewar container in the radial-axial plane and radial-circumferential plane, respectively, in cylindrical coordinates.

IX. Numerical Simulations of Sloshing Dynamics for the Operating GP-B Spacecraft

Computer simulations of sloshing dynamics applicable to orbital GP-B spacecraft have been carried out during the time period of the present research contract supported by the NASA grant NAG8-938. Results of the research are published in the following scientific journals:

(1) Hung, R. J., Lee, C. C., and Leslie, F. W., Effect of the Baffle on the Spacecraft Fluid Propellant Viscous Stress and Moment Fluctuations, Transactions of the Japan Society for Aeronautical and Space Sciences, 35, 187-207, 1993.

(2) Hung, R. J., and Shyu, K. L., Suction Dip, Liquid Residual and Slosh Wave Excitation During Liquid Draining in Microgravity, Advances in Space Research, 13(7), 147-154, 1993.

(3) Hung, R. J., and Shyu, K. L., Liquid Settlement, Resettlement,

Slosh Wave Excitation and Geyser Motion During Reorientation in Microgravity, Advances in Space Research, 13(7), 155-163, 1993.

(4) Hung, R. J., Lee, C. C., and Leslie, F. W., Effect of the Baffle on the Asymmetric Gravity-Jitter Excited Slosh Waves and Spacecraft Moment and Angular Momentum Fluctuations, Journal of Aerospace Engineering, (United Kingdom), 207, 105-120, 1993.

(5) Hung, R. J., and Pan, H. L., Asymmetric Slosh Wave Excitation in Liquid-Vapor Interface Under Microgravity, Acta Mechanica Sinica, 9(4), 298-311, 1993.

(6) Hung, R. J., and Lee, C. C., Effect of the Baffle on On-Orbit Spacecraft Fluid System Angular Momentum Fluctuations and Action of Viscous Stress Moment Exerted on the Container, Proceedings of National Science Council (A), 17, 214-235, 1993.

(7) Hung, R. J., and Pan, H. L., Differences in Gravity Gradient and Gravity Jitter-Excited Slosh Waves in Microgravity, Transactions of the Japan Society for Aeronautical and Space Sciences, 36, 153-169, 1993.

(8) Hung, R. J., and Shyu, K. L., Liquid Resettlement and Slosh Wave Excitation During Fluid Reorientation in Microgravity, Acta Astronautica, 27, in press, 1994.

(9) Hung, R. J., and Pan, H. L., Gravity Gradient or Gravity Jitter Induced Viscous Stress and Moment Fluctuations in Microgravity, Fluid Dynamics Research, 14(1), 29-51, 1994.

(10) Hung, R. J., and Pan, H. L., Cryogenic Helium System Angular Momentum and Moment Fluctuations Driven by Gravity Gradient Acceleration in Microgravity, Advances in Cryogenic Engineering,

39, 231-240,1994.

(11) Hung, R. J., and Lee, C. C., Effect of the Baffle on the Cryogenic Helium Container Angular Momentum and Moment Fluctuations Due to Asymmetric Gravity Jitter Excited Slosh Waves, Advances in Cryogenic Engineering, 39, 261-270, 1994.

(12) Hung, R. J., and Pan, H. L., Gravity Gradient Induced Viscous Stress and Moment Fluctuations of Cryogenic Helium System in Microgravity, Advances in Cryogenic Engineering, 39, 241-250, 1994.

(13) Hung, R. J., and Shyu, K. L., Cryogenic Liquid Hydrogen Suction Dip and Slosh Wave Excitation During Draining in Microgravity, Advances in Cryogenic Engineering, 39, 219-229, 1994.

(14) Hung, R. J., and Lee, C. C., Effect of the Baffle on the Cryogenic Helium Container Viscous Stress and Moment Fluctuations in Microgravity, Advances in Cryogenic Engineering, 39, 251-260, 1994.

(15) Hung, R. J., Lee, C. C., and Leslie, F. W., Dynamic Characteristics of the Partially Filled Rotating Dewar of the Gravity Probe-B Spacecraft, Acta Astronautica, 32(3), 199-209, 1994.

(16) Hung, R. J., and Lee, C. C., Effect of Baffle on Gravity Gradient Acceleration Excited Slosh Waves and Associated Viscous Stress Force Activated Spacecraft Dynamic Fluctuations, Aeronautical Journal (Royal Aeronautical Society of United Kingdom), in press, 1994.

(17) Hung, R. J., Lee, C. C., and Leslie, F. W., Dynamics of Gravity Probe-B Spacecraft Due to Gravity Jitter Induced Cryogenic Helium Disturbances in Rotating Dewar, Advances in Space Research, 14(5), 115-122, 1994.

(18) Hung, R. J., Pan, H. L., and Leslie, F. W., Fluid System Angular Momentum and Moment Fluctuations Driven by Gravity Gradient or Gravity Jitter in

Microgravity, Journal of Flight Sciences and Space Research (Zeitschrift fur Flugwissenschaften und Weltraumforschung), 18, 195-202, 1994.

(19) Hung, R. J., and Pan, H. L., Mathematical Formulation of Gravity Gradient and Gravity Jitter Accelerations Acting on the Fluid Systems of On-Orbit Orbital Spacecraft, Proceedings of National Science Council (A), 18(3), 236-247, 1994.

(20) Hung, R. J., and Pan, H. L., Numerical Modeling of Bubble Oscillations in Microgravity, Scientific Computing and Automation, 10(6), 21-25, 1994.

(21) Hung, R. J., and Pan, H. L., Turn-Around Gravity Jitter Excited Slosh Waves and Their Effects on Angular Momentum and Viscous Stress Exerted on Spacecraft, Proceedings of National Science Council,(A), 18, 353-370, 1994.

(22) Hung, R. J., and Shyu, K. L., Liquid Hydrogen Suction Dip and Slosh Wave Excitation During Draining Under Normal and Reduced Gravity Environments, Transactions of the Japan Society for Aeronautical and Space Sciences, 36, 225-248, 1994.

(23) Hung, R. J., Pan, H. L., and Long, Y. T., Sloshing Dynamics Modulated Cryogenic Helium Fluids Driven by Gravity Gradient or Jitter Accelerations Associated with Slew Motion in Microgravity, Acta Mechanica Sinica, 10, in press, 1994.

(24) Hung, R. J., and Lee, C. C., Effect of Baffle on Gravity Gradient Acceleration Excited Slosh Waves in Microgravity, Journal of Spacecraft and Rockets, 31, in press, 1994.

(25) Hung, R. J., Pan, H. L., and Long, Y. T., Peculiar Behavior of Helium II Disturbances Due to Sloshing Dynamics Driven by Jitter Accelerations Associated With Slew Motion in Microgravity, Cryogenics,34(8), 641-648, 1994.

(26) Hung, R. J., Long, Y. T., and Pan, H. L., Sloshing Dynamics Induced Angular Momentum Fluctuations Driven by Jitter Accelerations Associated with Slew Motion in Microgravity, Transactions of the Japan Society for Aeronautical and Space Sciences,37, 217-233,1994.

(27) Hung, R. J., and Pan, H. L., Sloshing Dynamics Modulated Fluid Angular Momentum and Moment Fluctuations Driven by Orbital Gravity Gradient and Jitter Accelerations in Microgravity, Applied Scientific Research Journal (International Journal of the Applications of Fluid Dynamics),in press, 1994.

(28) Hung, R. J., and Lee, C. C., Effect of Baffles on Imbalance Bubble Configuration Due to Sloshing Dynamics Driven by Gravity Gradient Acceleration in Microgravity, Canadian Aeronautics and Space Journal, 40, 185-202, 1994.

(29) Hung, R. J., and Shyu, K. L., Liquid Hydrogen Shut-Off Geyser Excitation Induced by Sloshing Dynamics During Draining in Microgravity. Aeronautical Journal (Royal Aeronautical Society of United Kingdom), in press, 1994.

(30) Hung, R. J., and Lee, C. C., Effect of Baffles on Sloshing Modulated Fluid Force and Torque Fluctuations on the Dewar Driven by Gravity Gradient Acceleration in Microgravity, Applied Scientific Research Journal, (International Journal of the Application of Fluid Dynamics),in press, 1994.

(31) Hung, R. J., and Pan, H. L., Fluid Force Activated Spacecraft Dynamics Driven by Gravity Gradient and Jitter Accelerations, Journal of Guidance, Control and Dynamics, 17, in press, 1994.

(32) Hung, R. J., and Pan, H. L., Simulation of Sloshing Dynamics Induced Forces and Torques Actuated on Dewar Container Driven by Gravity Gradient and Jitter Accelerations in Microgravity, Journal of Simulation Practice and Theory, in press, 1994.

(33) Hung, R. J., and Pan, H. L., Effect of Baffle on Sloshing Modulated Torques Responsed to Orbital Accelerations in Microgravity, Journal of Spacecraft and Rockets, 31, in press, 1994.

(34) Hung, R. J., Tsao, Y. D., and Spaulding, G. F., Gravity Effect on the Lymphocyte Deformation Through Cell Shape Change, Proceedings of National Science Council, (C), 17, in press, 1994.

(35) Hung, R. J., and Pan, H. L., Characteristics of Spin-Up Cryogenic Helium Bubble Encirclement Around Inner Column of Dewar Container in Microgravity, Advances in Space Research, 14, in press, 1994.

(36) Hung, R. J., Tsao, Y. D., and Spaulding, G. F., Time Sequence Evolution of Human Cell Deformation in Micro- and Hypergravity, Advances in Space Research, 14, in press, 1994.

(37) Hung, R. J., and Long, Y. T., Baffle Effect of Cryogenic Helium Sloshing Dynamics In Response to Lateral Impulsive Acceleration in Microgravity, Cryogenics, in press, 1994.

(38) Hung, R. J., and Pan, H. L, Rotational Speed and Wrapping of Different Size Cryogenic Helium Bubbles Around a Dewar Well in Microgravity, Aeronautical Journal (Royal Aeronautical Society of United Kingdom), in press, 1994.

(39) Hung, R. J., and Pan, H. L., Simulation of Bubble Spin-Up and Spin-Down in Microgravity, Scientific Computing and Automation, 10, in press, 1994.

(40) Hung, R. J., and Pan, H. L., Mathematical Modelling of Bubble Sloshing Dynamics for Cryogenic Liquid Helium in Orbital Spacecraft Dewar Container, Applied Mathematical Modelling, in press, 1994.

(41) Hung, R. J., and Pan, H. L., Sloshing Modulated Liquid-Vapor Interface Fluctuations Activated by Orbital Accelerations Associated with Spinning and/or Slew Motions, Journal of Colloid and Interface Science, in press, 1994.

(42) Hung, R. J., and Pan, H. L., Orbital Spacecraft Cryogenic Helium Dewar

Sloshing Dynamics Driven by Gravity Gradient Acceleration Associated with Slew Motion, Japan Society of Mechanical Engineers International Journal /Fluid and Thermal Engineering, in press, 1994.

(43) Hung, R. J., and Pan, H. L., Combined Gravity Gradient and Jitter Accelerations Acting on Liquid-Vapor Interface Oscillations in Reduced Gravity, International Journal of Mechanical Sciences, in press, 1994.

In addition to the publication in the scientific journals, we have also published the research results in the national and international scientific conferences. The listing of the papers published in the conference proceedings are as follows:

(1) Hung, R. J., Lee, C. C., and Leslie, F. W., Effect of the Baffle on Asymmetric Gravity Jitter Excited Slosh Waves in Microgravity, AIAA Paper, No. 93-0913, pp. 11, 1993.

(2) Hung, R. J., and Pan, H. L., Cryogenic Helium System Angular Momentum and Moment Fluctuations Driven by Gravity Gradient Acceleration in Microgravity, Cryogenic Engineering Conference Proceedings, pp. 11, 1993.

(3) Hung, R. J., and Lee, C. C., Effect of the Baffle on the Cryogenic Helium Container Viscous Stress and Moment Fluctuations in Microgravity, Cryogenic Engineering Conference Proceedings, pp. 11, 1993.

(4) Hung, R. J., and Pan, H. L., Gravity Gradient Induced Viscous Stress and Moment Fluctuations of Cryogenic Helium System in Microgravity, Cryogenic Engineering Conference Proceedings, pp. 11, 1993.

(5) Hung, R. J., and Shyu, K. L, Cryogenic Liquid Hydrogen Suction Dip and Slosh Wave Excitation During Draining in Microgravity, Cryogenic Engineering Conference Proceedings, pp. 11, 1993.

(6) Hung, R. J., and Lee, C. C., Effect of the Baffle on the Cryogenic Helium

Container Angular Momentum and Moment Fluctuations Due to Asymmetric Gravity Jitter Excited Slosh Waves, Cryogenic Engineering Conference Proceedings, pp. 11, 1993.

(7) Hung, R. J., and Chen, A. J., VHF Radar and Doppler Sounder Remote Sensing of Severe Weather-Related Thermospheric and Mesospheric Disturbances Over Taiwan, Proceedings of First Pacific International Conference on Aerospace Science and Technology, Vol. II, 899-903, 1993.

(8) Hung, R. J., and Leslie, F. W., Characteristics of Gravity Probe-B Spacecraft Cryogenic Propellant Management, Proceedings of First Pacific International Conference on Aerospace Science and Technology, Vol. III, 1417-1423, 1993.

(9) Hung, R. J., and Pan, H. L., Acting of Gravity Gradient and Gravity Jitter Accelerations on the On-Orbit Orbital Spacecraft, Proceedings of First Pacific International Conference on Aerospace Science and Technology, Vol. I, 490-497, 1993.

(10) Hung, R. J., and Shyu, K. L., Liquid Propellant Residual and Shut-Off in Spacecraft Propulsion System, Proceedings of First Pacific International Conference on Aerospace Science and Technology,Vol. III, 1396-1405, 1993.

(11) Hung, R. J., and Long, Y. T., Mathematical Model of Variable Polarity Plasma Arc Welding Process and Fabrication of Space Systems, Proceedings of First Pacific International Conference on Aerospace Science and Technology, Vol. II, 605-615, 1993.

(12) Hung, R. J., and Lee, C. C., Effect of the Baffle on On-Orbit Spacecraft Angular Momentum and Viscous Moment Exerted on Propellant System, Proceedings of First Pacific International Conference on Aerospace Science and Technology, Vol. III, 1406-1416, 1993.

(13) Hung, R. J., and Shyu, K. L., Vapor ingestion, Liquid Residual and Slosh Wave Excitation During Two-Phase Flow Drainage and Shut-Off in Microgravity, AIAA Paper, No. 94-0703, pp. 11, 1994.

(14) Hung, R. J., and Pan, H. L., Liquid-Vapor Interface Fluctuations Induced by Gravity Gradient and Jitter Accelerations in Microgravity, AIAA Paper, No. 94-0439, pp. 12, 1994.

(15) Hung, R. J., Overviews of GP-B Liquid Helium Dewar Sloshing Analysis, Workshop for NASA Computational Fluid Dynamic Applications in Rocket Propulsion, pp. 11, 1994.

(16) Hung, R. J., and Pan, H. L., Characteristics of Spin-Up Cryogenic Helium Bubble Encirclement Around Inner Column of Dewar Container in Microgravity, COSPAR, 30, pp. 15, 1994.

(17) Hung, R. J., and Tsao, Y. D., Time Sequence Evolution of Human Cell Deformation in Microgravity,COSPAR, 30, PP. 14, 1994.

(18) Hung, R. J., and Pan, H. L., Spin-Up of Partially Filled Fluids with Bubble in Microgravity, AIAA Paper, No. 94-2305, pp. 11, 1994.

(19) Hung, R. J., Tsao, Y. D., and Spaulding, G. F., Dynamics of Human Cell Deformation in Microgravity,AIAA Paper, No. 94-2403, pp. 12, 1994.

(20) Hung, R. J., and Long, Y. T., Sloshing Induced Liquid Feedback Force and Torque Fluctuations Associated with Slew Motion in Microgravity, Symposium of Space Sciences and Technology, (Beijing,China), pp. 12, 1994.

(21) Hung, R. J., and Pan, H. L., Effect of Baffle on the Spacecraft Fluid System Sloshing Dynamics Induced Liquid Feedback Force and Torque Fluctuations Driven by Orbital Accelerations, Symposium of Space Sciences and Technology, (Beijing, China), pp. 10, 1994.

(22) Hung, R. J., and Long, Y. T., Impulse Driven Propellant Sloshing Dynamics

in Microgravity, Symposium of Space Science and Technology, (Beijing, China), pp. 10, 1994.

(23) Hung, R. J., and Pan, H. L., Characteristics of Bubble Spin-Up in Spacecraft Partially Filled Liquid Propellant in Rotating Dewar, Symposium on Space Science and Technology, (Beijing, China), pp. 15, 1994.

(24) Hung, R. J., and Long, Y. T., Effect of Baffle on the Cryogenic Helium Sloshing Dynamics Driven by Axial Impulse, Symposium on Space Science and Technology, (Beijing, China), pp. 13, 1994.

(25) Hung, R. J., and Pan, H. L., Cryogenic Helium Sloshing Dynamics Driven by Gravity Gradient and G-Jitter Accelerations in Microgravity, Symposium on Space Science and Technology, (Beijing, China), pp. 15, 1994.

Acknowledgement

The authors appreciate the support received from the National Aeronautics and Space Administration through the NASA Grant NAG8-938. They would like to express their gratitude to Richard A. Potter and Fred W. Leslie of NASA/Marshall Space Flight Center for the stimulating discussions during the course of the present study.

References

Avduyevsky V. S. (editor), Scientific Foundations of Space Manufacturing, MIR, Moscow, USSR 1984.

Everitt, F. Ed., Testing Einstein With Orbiting Gyroscopes - Gravity Probe-B, pp. 28, Stanford University, Palo Alto, CA, 1990.

Forward, R. L., Flattening Space-Time Near the Earth, Physical Review, Series D, Vol. 26, pp. 735-744, 1982.

Hoare, F. E., Jackson, L. C., and Kurti, N., Experimental Cryogenics; Liquid Helium II, Butterworths, London, U.K. (1961).

Hung, R. J., Superfluid and Normal Fluid Helium II in a Rotating Tank Under Low and Microgravity Environments, Proceedings of National Science Council, Series (A), Vol. 14, pp. 289-29, 1990.

Hung, R. J., and Lee, C. C., Characteristics and Behaviors of Gravity Probe-B Spacecraft Propulsion System, Proceed. National Science Council (A), 16, pp. 339-352, 1992.

Hung, R. J., Lee, C. C., and Leslie, F. W., Dynamics of Gravity Probe-B Spacecraft Due to Gravity Jitter Induced Cryogenic Helium Disturbances in Rotating Dewar, Advances in Space Research, Vol. 14, 115-122, 1994a.

Hung, R. J., Lee, C. C., and Leslie, F. W., Effect of G-Jitters on the Stability of Rotating Bubble Under Microgravity Environment, Acta Astronautica, Vol. 21, pp. 309-321, 1990a.

Hung, R. J., Lee, C. C., and Leslie, F. W., Gravity-Jitter Response Slosh Waves Excitation on the Fluid Rotating Dewar, Advances in Space Research, Vol. 11(7), pp. 201-208, 1991d.

Hung, R. J., Lee, C. C., and Leslie, F. W., Gravity-Jitter Effected Slosh Waves on the Stability of Rotating Bubble Under Microgravity Environment,

Advances in Space Research, Vol. 11(7), pp. 209-216, 1991e.

Hung, R. J., Lee, C. C., and Leslie, F. W., Slosh Wave Excitation in a Partially Filled Rotating Tank Due to Gravity Jitters in a Microgravity Environment, Acta Astronautica, Vol. 25, pp. 523-551, 1991f.

Hung, R. J., Lee, C. C., and Leslie, F. W., Response of Gravity Level Fluctuations on the Gravity Probe-B Spacecraft Propellant System, Journal of Propulsion and Power, Vol. 7, pp. 556-564, 1991g.

Hung, R. J., Lee, C. C., and Leslie, Slosh Wave Excitation of Cryogenic Liquid Helium in Gravity Probe-B Rotating Dewar, Advances in Cryogenic Engineering, 37, 1281-1290, 1991j.

Hung, R. J., Lee, C. C., and Leslie, F. W., Gravity Jitter Excited Cryogenic Liquid Slosh Waves in Microgravity Environment, Advances in Cryogenic Engineering, 37, 1291-1302, 1991c.

Hung, R. J., Lee, C. C., and Leslie, F. W., Spacecraft Dynamical Distribution of Fluid Stresses Activated by Gravity Jitter Induced Slosh Waves, Journal of Guidance, Control and Dynamics, Vol. 15, pp. 817-824, 1992c.

Hung, R. J., Lee, C. C., and Leslie, F. W., Similarity Rules in Gravity Jitter-Related Spacecraft Liquid Propellant Slosh Waves Excitation, Journal of Fluids and Structures, Vol. 6, pp. 493-522, 1992d.

Hung, R. J., Lee, C. C., and Leslie, F. W., Effect of the Baffle on the Spacecraft Fluid Propellant Viscous Stress and Moment Fluctuations, Transaction of the Japan Society for Aeronautical and Space Sciences, 35, 187-207, 1993a.

Hung, R. J., Lee, C.C., and Leslie, F. W., Effect of the Baffle on the Asymmetric Gravity-Jitter Excited Slosh Waves and Spacecraft Moment and Angular Momentum Fluctuations, Journal of Aerospace Engineering (United Kingdom),

207,105-120 1993b.

Hung, R. J., Lee, C. C., and Shyu, K. L., Reorientation of Rotating Fluid in Microgravity Environment With and Without Gravity Jitters, Journal of Spacecraft and Rockets, Vol. 28, pp. 71-79, 1991h.

Hung, R. J., and Leslie, F. W., Bubble Shapes in a Liquid-Filled Rotating Container Under Low Gravity, Journal of Spacecraft and Rockets, Vol. 25, pp. 70-74, 1988.

Hung, R. J., Pan, H. L., and Leslie, F. W. Gravity Gradient or Gravity Jitter Induced Viscous Stress and Moment Fluctuations in Microgravity, Fluid Dynamics Research,14(1), 29-51, 1993d.

Hung, R. J., and Pan, H. L., Asymmetric Slosh Wave Excitation in Liquid-Vapor Interface Under Microgravity, Acta Mechanica Sinica,9(4), 298-311,1993.

Hung, R. J., and Shyu, K. L., Cryogenic Hydrogen Reorientation and Geyser Initiation at Various Liquid-Filled Levels in Microgravity, Advances in Space Research, Vol. 11(7), pp. 217-226, 1991a.

Hung, R. J., and Shyu, K. L., Cryogenic Liquid Hydrogen Reorientation Activated by High Frequency Impulsive Reverse Gravity Acceleration of Geyser Initiation, Microgravity Quarterly, Vol. 1(2), pp. 81-92, 1991b.

Hung, R. J., and Shyu, K. L., Space-Based Cryogenic Liquid Hydrogen Reorientation Activated by Low Frequency Impulsive Reverse Gravity Thruster of Geyser Initiation, Acta Astronautica, Vol. 25, pp. 709-719, 1991c.

Hung, R. J., and Shyu, K. L., Constant Reverse Thrust Activated Reorientation of Liquid Hydrogen with Geyser Initiation, Journal of Spacecraft and Rockets, Vol. 29, pp. 279-285, 1992a.

Hung, R. J., and Shyu, K. L., Excitation of Slosh Waves Associated with Low Frequency Impulsive Reverse Gravity Acceleration of Geyser Initiation, Acta

Astronautica, Vol. 26, pp. 425-433, 1992b.

Hung, R. J., and Shyu, K. L., Medium Frequency Impulsive Thrust Activated Liquid Hydrogen Reorientation with Geyser, Journal of Propulsion and Power, Vol. 8, pp. 987-994, 1992c.

Hung, R. J., and Shyu, K. ., Suction Dip, Liquid Residual and slosh Wave Excitation during Liquid Draining in Microgravity, Advances in Space Research, 13(7), 147-154, 1993a.

Hung, R. J., and Shyu, K. L., Liquid Settlement, Resettlement, Slosh Wave Excitation and Geyser Motion During Reorientation in Microgravity, Advances in Space Research, 13(7), 155-163, 1993b.

Hung, R. J., and Shyu, K. L., Liquid Resettlement and Slosh Wave Excitation During Fluid Reorientation in Microgravity, Acta Astronautica, 28, in press, 1994.

Hung, R. J., Shyu, K. L., and Lee, C. C., Slosh Wave Excitation Associated with High Frequency Impulsive Reverse Gravity Acceleration of Geyser Initiation, Microgravity Quarterly, Vol. 1(3), pp. 125-133, 1991i.

Hung, R. J., Shyu, K. L., and Lee, C. C., Cryogenic Liquid Resettlement Activated by Impulsive Thrust in Microgravity Environment, Advances in Cryogenic Engineering, 37, 1313-1326, 1991a.

Hung, R. J., Shyu, K. L., and Lee, C. C., Slosh Wave Excitation Due to Cryogenic Liquid Reorientation in Space-Based Propulsion System, Advances in Cryogenic Engineering, 37, 1303-1312, 1991b.

Hung, R. J., Shyu, K. L., and Lee, C. C., Medium Frequency Impulsive Thrust Excited Slosh Waves During Propellant Reorientation with Geyser, Journal of Propulsion and Power, Vol. 8, pp. 778-785, 1992a.

Hung, R. J., Shyu, K. L., and Lee, C. C., Liquid Hydrogen Slosh Wave Excited by

Constant Reverse Gravity Acceleration of Geyser Initiation, Journal of Spacecraft and Rockets, Vol. 29, pp. 523-528, 1992b.

Hung, R. J., Tsao, Y. D., Hong, B. B., and Leslie, F. W., Time Dependent Dynamical Behavior of Surface Tension on Rotating Fluids Under Microgravity Environment, Advances in Space Research, Vol. 8(12), pp. 205-213, 1989d.

Hung, R. J., Tsao, Y. D., Hong, B. B., and Leslie, F. W., Dynamics of Surface Tension in Microgravity Environment, Progress in Aeronautics and Astronautics, Vol. 127, pp. 124-150, 1990b.

Hung, R. J., Tsao, Y. D., Hong, B. B., and Leslie, F. W., Dynamical Behavior of Surface Tension on Rotating Fluids in Low and Microgravity Environments, International Journal for Microgravity Research and Applications, Vol. 11, pp. 81-95, 1989a.

Hung, R. J., Tsao, Y. D., Hong, B. B., and Leslie, F. W., Axisymmetric Bubble Profiles in a Slowly Rotating Helium Dewar Under Low and Microgravity Environments, Acta Astronautica, Vol. 19, pp. 411-426, 1989b.

Hung, R. J., Tsao, Y. D., Hong, B. B., and Leslie, F. W., Bubble Behaviors in a Slowly Rotating Helium Dewar in Gravity Probe-B Spacecraft Experiment, Journal of Spacecraft and Rockets, Vol. 26, pp. 167-172, 1989c.

Kamotani, Y., Prasad, A., and Oastrach, S., Thermal Convections in an Enclosure Due to Vibrations Aboard a Spacecraft, AIAA Journal, Vol. 19, pp. 511-516, 1981.

Landau, L. D., and Lifshitz, Fluid Mechanics, Pergamon Press, London, pp. 1-656, 1959.

Leslie, F. W., Measurements of Rotating Bubble Shapes in a Low Gravity Environment, Journal of Fluid Mechanics, Vol. 161, pp. 269-275, 1985.

Mason, P., Collins, D., Petrac, D., Yang, L., Edeskuty, F., Schuch, A.,

and Williamson, K., The Behavior of Superfluid Helium in Zero Gravity, Proceedings 7th International Cryogenic Engineering Conferences, Surrey, England, Science and Technology Press, 1978.

Misner, C. W., Thorne, K. S., and Wheeler, J. A., Gravitation, W. H. Freeman Co., San Francisco, CA, pp. 1-1279, 1973.

Stanford Relativity Gyroscope Experiment (NASA Gravity Probe-B), Proceedings of Society of Photo-Optical Instrumentation Engineers, 619, pp. 1-165, Society of Photo-Optical Instrumentation Engineers, Bellingham, WA, 1986.

Weinberg, S., Gravitation and Cosmology - Principles and Applications of General Relativity, pp. 657, John Wiley and Sons, New York, 1972.

Wilks, J., The Properties of Liquid and Solid Helium, Clarendon Press, Oxford, U.K., 1967.

Wilkinson, D. T., Bender, P. I., Eardley, D. M., Gaisser, T. K., Hartle, J. B., Israel, M. H., Jones, L. W., Partridge, R. B., Schramm, D. N., Shapiro, I. I., Vessort, R. F. C., and Wagoner, R. V., Gravitation, Cosmology and Cosmic Ray Physics, Physics Today, 39, 43-46, 1986.

Figure Captions

Figure 1 GP-B spacecraft coordinate systems with azimuth angle ψ_E from spacecraft mass center to the center of the Earth. Coordinate (x", y", z") for slew motion and coordinate(x, y, z) for fluid mechanics computation.

Figure 2 Geometry of the GP-B dewar container with the coordinate system perpendicular and tangential to the container wall. (A) Geometry in r-z plane and (B) Geometry in r-θ plane.

Figure 3 Geometry of the GP-B dewar container with baffle-boards and their locations. (A) Geometry in r-z plane and (B) Geometry in r-θ plane.

Figure 4 The GP-B module showing main elements of liquid helium dewar, probe and baffle-boards.

Figure 5 Distribution of grid points in the (A) Radial-axial plane, and (B) the radial-circumferential plane of the cylindrical coordinates for the GP-B dewar tank.

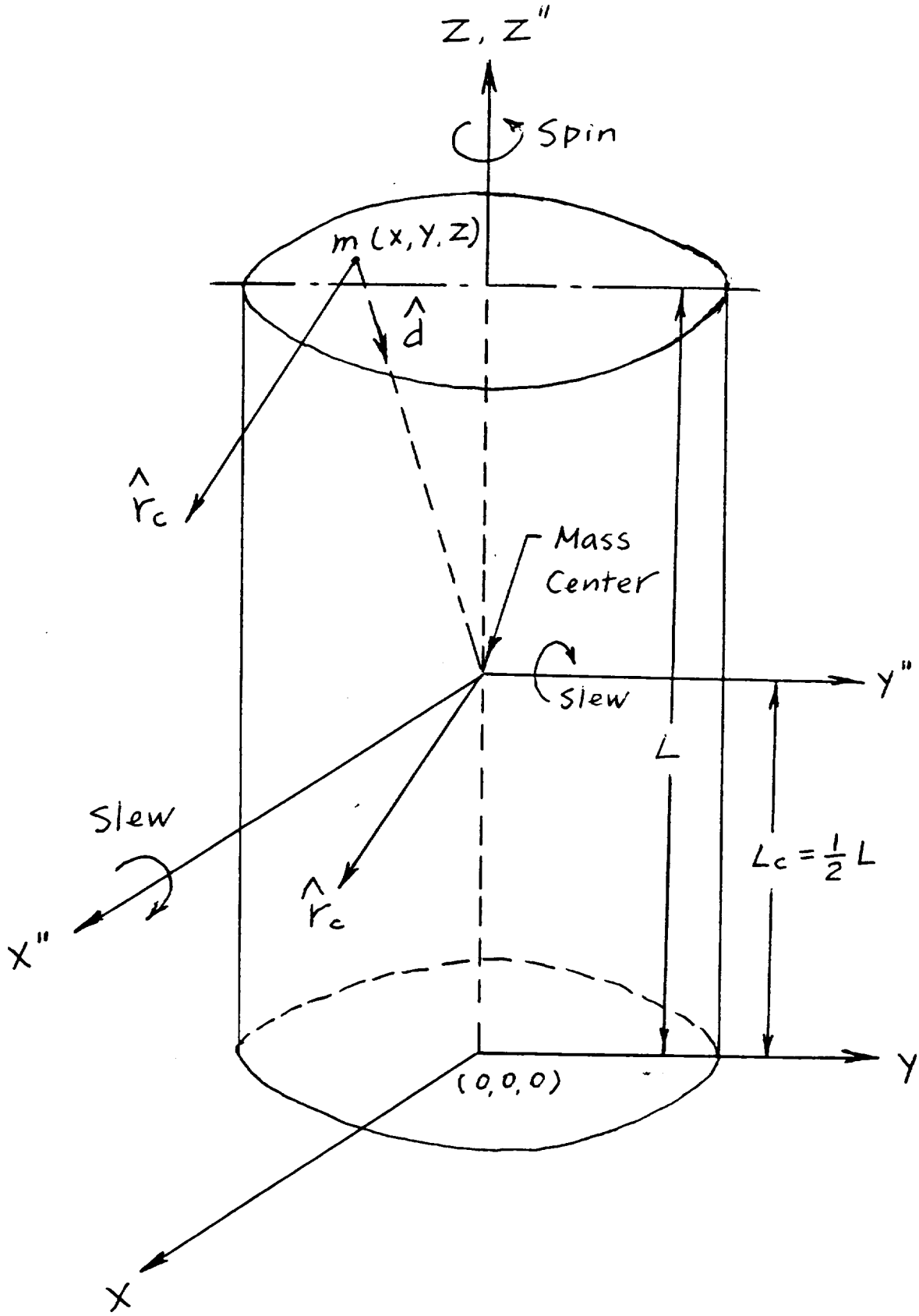
Z, Z"
Spin
m (x, Y, Z)
$\hat{d}$
$\hat{r}_c$
Mass
Center
Slew
Y"
L
Slew
X"
$\hat{r}_c$
$L_c = \frac{1}{2} L$
Y
(0, 0, 0)
X

Fig. 1

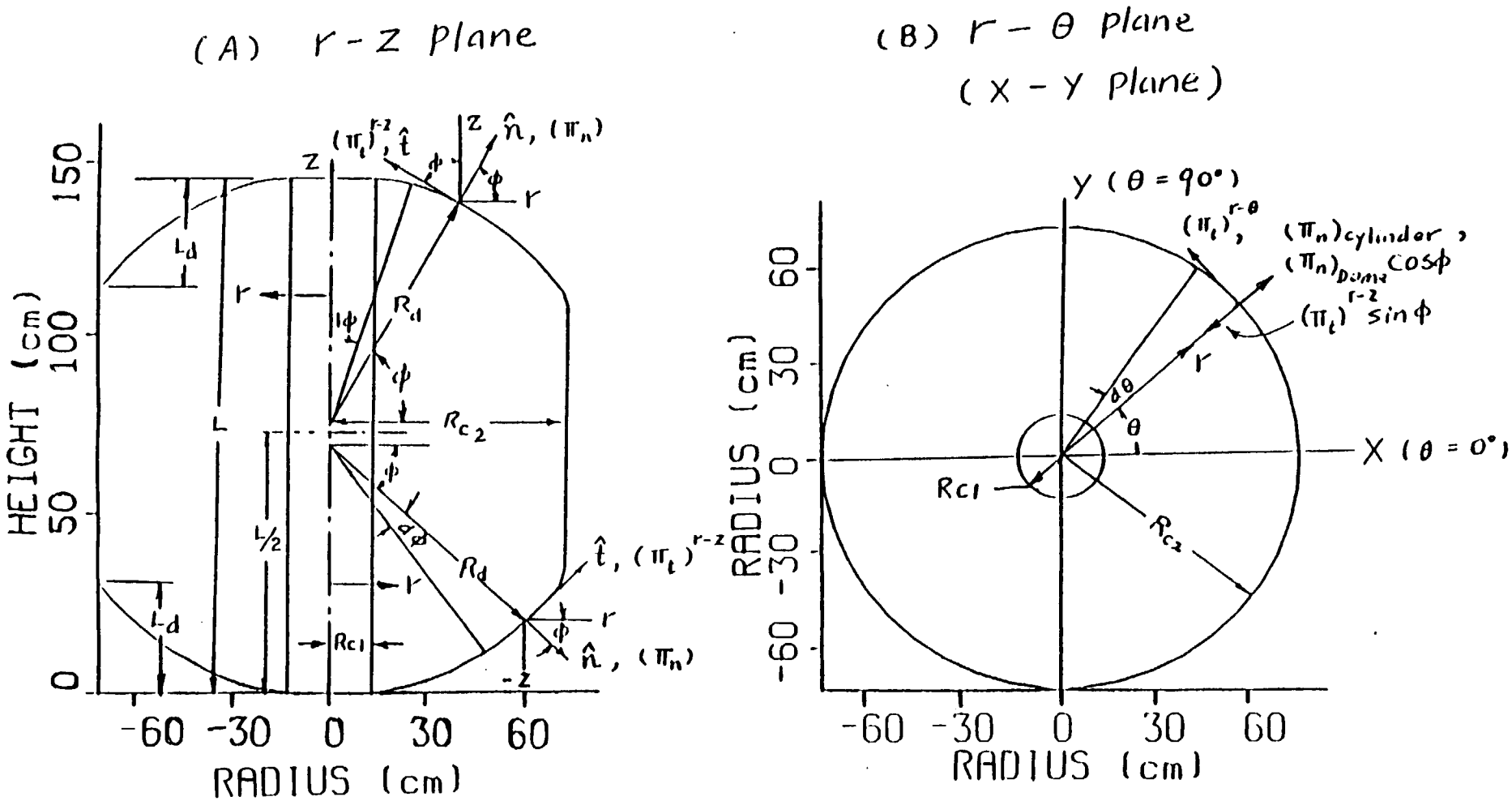
(A) r - z plane
HEIGHT (cm)
150
100
50
0
-60 -30 0 30 60
RADIUS (cm)
z
r
L_d
L
L/2
R_{c_1}
R_{c_2}
R_d
ϕ
$\hat{n}$, (π_n)
$\hat{t}$, $(\pi_t)^{r-z}$
-z
(B) r - θ plane
(x - y plane)
y (θ = 90°)
X (θ = 0°)
RADIUS (cm)
60
30
0
-30
-60
$(\pi_t)^{r-\theta}$,
$(\pi_n)_{cylinder}$,
$(\pi_n)_{Dome}\cos\phi$
$(\pi_t)^{r-z}\sin\phi$
$d\theta$
θ
R_{c_1}
R_{c_2}

Fig. 2

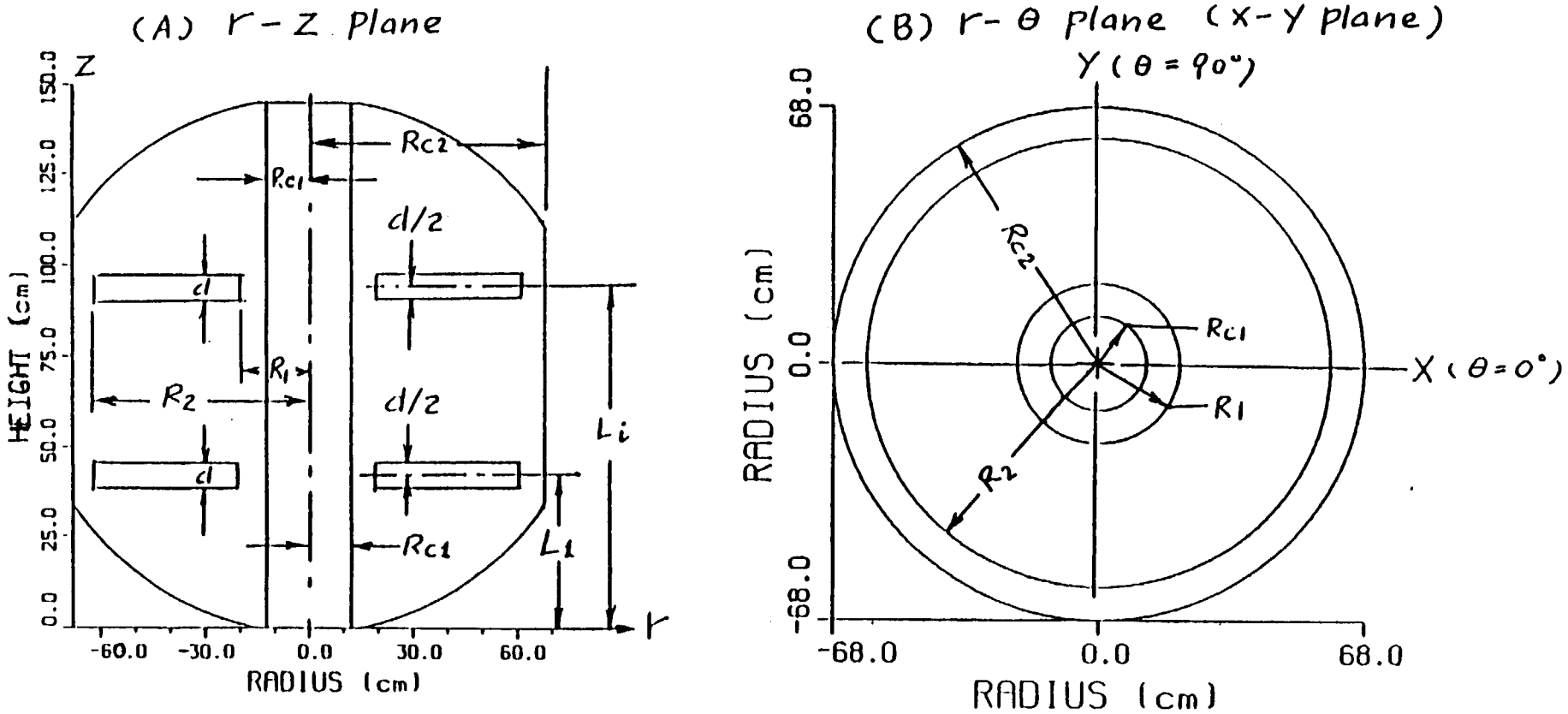
(A) r-Z Plane
Z
HEIGHT (cm)
150.0
125.0
100.0
75.0
50.0
25.0
0.0
Rc2
Rc1
d/2
d
R1
R2
d/2
d
Li
L1
Rc1
r
-60.0
-30.0
0.0
30.0
60.0
RADIUS (cm)
(B) r-θ Plane (X-Y Plane)
Y (θ = 90°)
68.0
0.0
-68.0
RADIUS (cm)
Rc2
Rc1
R1
R2
X (θ = 0°)
-68.0
0.0
68.0
RADIUS (cm)

Fig. 3

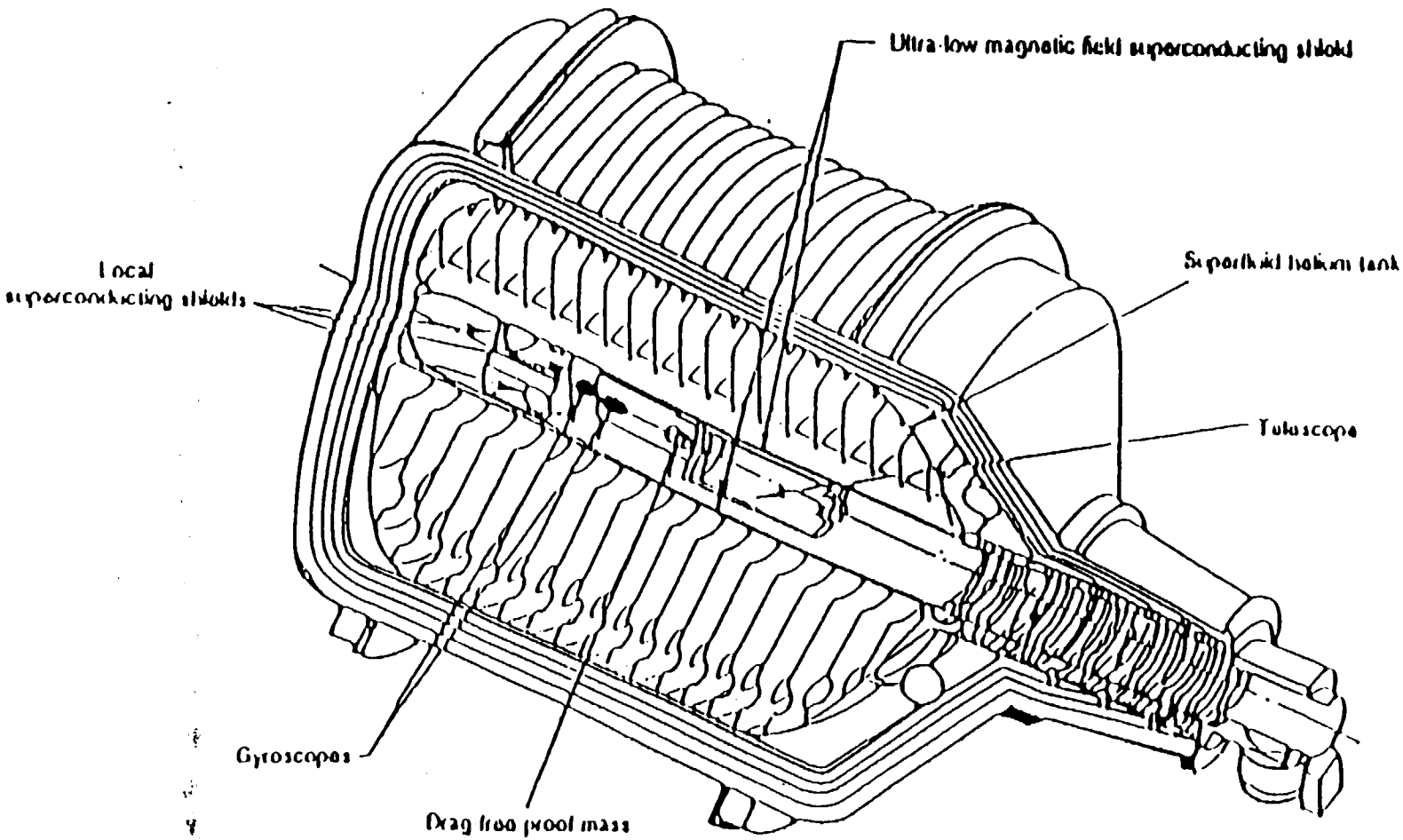
Ultra-low magnetic field superconducting shield
Local superconducting shields
Superfluid helium tank
Telescope
Gyroscopes
Drag free proof mass

Fig. 4

(A) r - z Plane
at θ = O°

(B) r - θ Plane
(x - y Plane)
at z = L/2

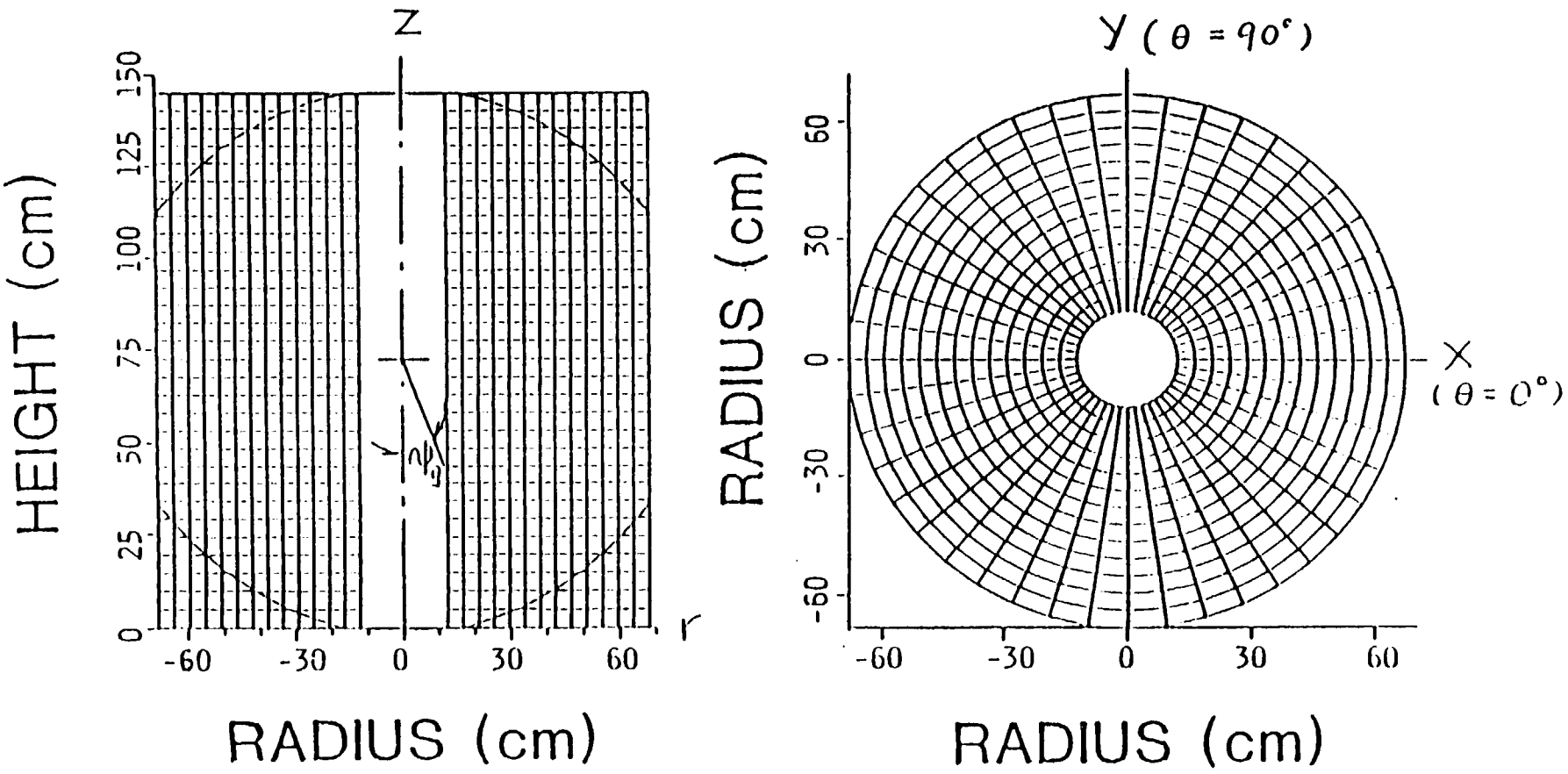

Fig. 5